FORM-F

COUNCIL OF SCIENTIFIC AND INDUSTRIAL RESEARCH
Human Resource Development Group
(Extra Mural Research Division)
CSIR Complex, Library Avenue, Pusa, New Delhi – 110012

FINAL TECHNICAL REPORT

1. Title of the scheme

A multiwavelength study of Active Galactic Nuclei and X-ray sources	Scheme No.: 03(1412)/17/EMR-II Date of Commencement : 28/07/2017 Date of termination : 31/12/2021

2. Name and address of Principal Investigator

Dr Rupjyoti Gogoi,
Assistant Professor,
Department of Physics,
Tezpur University, Napaam-784028.

3. Name of Sponsoring laboratory of CSIR (If applicable)

NA

4. Total grant sanctioned and expenditure during the entire tenure

	Amount Sanctioned	Expenditure
Staff	8,25,000/	6,70,548/
Contingency	1,91,667/	1,66,083/
Equipment	2,00,000/	1,97,138/
Overhead		11,848/
Total	12,16,667/	10,46,372/

5. Equipment(s) purchased out of CSIR grant

Name	Cost
1.Workstation : Make & Model: DELL Precision Tower 3620 (with 22'' Monitor)	99,000 + 5% GST = 103950.00
2. Desktop Computer: Desktop with Windows, Make & Model: LENOVO Think Centre M910 Intel i5 7th Gen Processor 3.0 Ghz/Windows 10 Pro/4GB DDR4/ Intel Q270 Chipset or better/500GB SATA HDD/DVD Writer/Integrated HD Graphics/Gigabit Ethernet/19.5 LED Monitor/Std Keyboard/Optical Mouse.	42,750 + 5% GST = 44,887.50
3. UPS Orion 2KVA On-Line UPS System with Inbuilt Isolation Transformer with 60 minutes Back-Up Time using 6*12V*42AH SMF Batteries, Rack & Interlinks	46,000+ 5% GST = 48,300.00

6. Research fellows associated with scheme

Name& Designation	Date of Joining	Date of leaving
Rukaiya Khatoon, Project JRF Current Position: Postdoctoral Fellow, North-West University, South Africa.	28/07/2017	31/12/2021

7. Name(s) of the fellow(s) who received Ph.D. by working in the scheme, along with the Title(s) of thesis:
Dr. Rukaiya Khatoon,
Thesis Title: Multiwavelength temporal study of blazars

8. List of research papers published/communicated, based on the research work done under the scheme (Name(s) of author(s), Title, Journal, Volume number, Year and Pages should be given for each paper published and a copy of each of them should be enclosed; reprints/copies of papers appearing after submission of FTR should also be sent to CSIR):

(1) "Correlations between X-ray spectral parameters of Mkn 421 using long-term Swift–XRT data", Rukaiya Khatoon, Zahir Shah, Jyotishree Hota, Ranjeev Misra, Rupjyoti Gogoi, Ananta C Pradhan, **Monthly Notices of the Royal Astronomical Society**, Volume 515, Issue 3, September 2022, Pages 3749–3759, https://doi.org/10.1093/mnras/stac1964

(2) "Temporal and spectral study of PKS 0208–512 during the 2019–2020 flare, Rukaiya Khatoon, Raj Prince, Zahir Shah, Sunder Sahayanathan, Rupjyoti Gogoi", **Monthly Notices of the Royal Astronomical Society**, Volume 513, Issue 1, June 2022, Pages 611–623, https://doi.org/10.1093/mnras/stac892

(3) "Flux Distribution Study of Mkn 421 with SPOL, RXTE and Fermi-LAT Telescopes", Rukaiya Khatoon, Zahir Shah, Raj Prince, Ranjeev Misra & Rupjyoti Gogoi, **Selected Progresses in Modern Physics**. Springer Proceedings in Physics, vol 265. Springer, Singapore. https://doi.org/10.1007/978-981-16-5141-0_13, Januaru 2022 (Part of the Springer Proceedings in Physics book series (SPPHY,volume 265))

(4) "Study of long-term flux and photon index distributions of blazars using RXTE observations", Rukaiya Khatoon, Zahir Shah, Ranjeev Misra and Rupjyoti Gogoi, **Monthly Notices of the Royal Astronomical Society**, Volume 491, Issue 2, January 2020, Pages 1934–1940, https://doi.org/10.1093/mnras/stz3108

(5) "The flux distribution of individual blazars as a key to understand the dynamics of particle acceleration", Atreyee Sinha, Rukaiya Khatoon, Ranjeev Misra, Sunder Sahayanathan, Soma Mandal, Rupjyoti Gogoi and Nilay Bhatt, **Monthly Notices of the Royal Astronomical Society: Letters**, Volume 480, Issue 1, October 2018, Pages L116–L120, https://doi.org/10.1093/mnrasl/sly136

9. Details of new apparatus or equipment designed or constructed during the investigation:
    Nil

10. The likely impact of the completed work on the scientific/technological potential in the country (this may be attached as Enclosure-I):

AstroSat, the first Indian space observatory, was launched on 28th September, 2015 and has been observing bright AGNs including Blazars over the last seven years. The multi-wavelength simultaneous observations in both X-rays and ultraviolet make AstroSat data, unique and valuable to test theories. We believe, one can pursue a detailed study of some of the sources presented in this work and use the results obtained from the flux and index distributions to shed light on the underlying radiative mechanisms of these enigmatic objects.

11. Is the research work done of some industrial or agricultural importance and whether patent(s) should be taken?
    No

12. How has the research work complemented the work of CSIR Laboratory that sponsored your scheme?
    NA

13. Detailed account of the work carried out in terms of the objective(s) of the project and how for they have been achieved; results and discussion should be presented in the manner of a scientific paper/project report in about 5000 words; and this should be submitted as Enclosure-II to this report.
 (Please refer to Enclosure II)

14. An abstract of research achievements in about 200-500 words, suitable for publication.
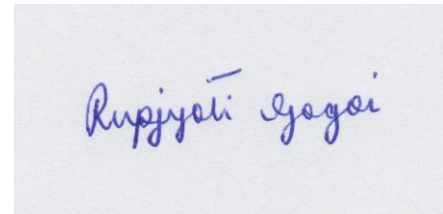
A compact core at the centre of a galaxy with luminosity $\geq 10^{44}$ ergs s^{-1} is known as active galactic nuclei (AGN). Blazars are the class of AGN for which the relativistic jet is aligned close to the line of sight of the observer. A physically motivated model is needed for a better understanding of intrinsic curvature seen in X-say spectrum of blazars. We have studied long term flux distributions of such sources and developed a numerical code to model the flux distribution. Then we have analyzed the flux and the photon spectral index light curves from the available Monitor of All-sky X-ray Image (MAXI) data in the X-ray band to see whether the observational results are consistent with the Theoretical/Numerical results. We have studied the effect of a Gaussian perturbation in the acceleration timescale on the observed spectrum. To model the emission scenario of blazars, we consider two-zones, one around the shock front where the acceleration of a mono energetic electron distribution takes place and the next down stream where they lose most of their energy through radiative processes. We have also studied the flux and the photon spectral index distributions of the blazar sources by using 16 years of Rossi X-ray

Timing Explorer (RXTE) archival data. Characterization of flux/index distribution and correlation study between the flux and photon index is also attempted.

We have produced one PhD student with this project, who is currently working as Postdoctoral researcher at North-West University of South Africa.

15. Mention here whether or not the unspent grant has been refunded to CSIR:
Yes, via a demand draft bearing number 847197, dated 12-05-2023.

Date: Signature of PI

Note: Final Technical Report is expected to be self-contained complete report of the work done.
Please do not leave any column unanswered.

Scheme number: 03(1412)/17/EMR-II

1 Objectives

1. To study the flux distribution of individual Blazars (special class of Active Galactic Nuclei) as a key to understand the dynamics of particle acceleration.

2. To study the Flux and Index distribution of different types of blazar sources with the Rossi X-ray Timing Explorer (RXTE) observation.

3. To study the X-ray SED modelling using Swift data.

2 Introduction

A compact core at the centre of a galaxy with luminosity $\geq 10^{44}$ ergs s^{-1} is known as Active Galactic Nuclei (AGN). They are bright at radio frequencies and their energy estimates show the minimum energy content of AGN to be $> 10^{60}$ erg (Burbidge). This huge energy reservoir is attributed to gravitational potential of super-massive black hole of mass $> 10^6 M_\odot$ accreting matter from its surroundings (Hoyle & Fowler). High resolution radio map of many AGNs show a well collimated jet with patterns moving at superluminal velocities. This along with the detection at gamma ray energies confirms that AGN possess relativistic jets powered by the central black hole.

Blazars are the class of AGN for which the relativistic jet is aligned close to the line of sight of the observer (Urry & Padovani 1995). In general, the mechanism powering these objects is thought to be the Synchrotron radiation followed by the Inverse Compton scattering in a beamed relativistic jet (Urry & Padovani 1995). Their broad band spectrum is predominantly non-thermal extending from radio to gamma-ray energies. Further they are characterized with rapid flux variations and high polarizations. Blazars have a double hump structure spectral energy distribution (SED) (Fossati et al. 1998), with low energy component peaking at optical/UV/soft X-ray energies, which is well established to be caused by synchrotron emission from relativistic electrons gyrating in the magnetic field of the jet, whereas the high energy component at gamma-ray energies can be attributed either to inverse Compton (IC) scattering of low-frequency photons (leptonic models) (Maraschi et al. 1992) or to hadronic cascades initiated in the jet. Blazars are further classified into BL Lacs and Flat Spectrum Radio Quasars (FSRQ) depending on the presence or absence of emission/absorption line features (Urry & Padovani 1995; Fan 2003). Based on the location of the peak frequency in the low energy component, BL Lac type objects are further classified into three subclasses namely, high energy peaked BL-Lac (HBL; $\nu_p > 10^{15.3}$ Hz), intermediate energy peaked BL-Lac (IBL; $10^{14} < \nu_p \leq 10^{15.3}$ Hz), and low energy peaked BL-Lac (LBL; $\nu_p \leq 10^{14}$ Hz).

The blazars light curves show an unpredictable luminosity variations over a broad range of time-scales ranging from minutes to years across the entire electro-magnetic spectrum. Modelling their long-term flux distribution can provide a clue about the nature of physical processes causing such variations. Typically when the flux variations are stochastic and linear, one would obtain a Gaussian distribution of fluxes with the width of the distribution determining the flux variation. However, if the stochastic flux variation is non-linear, one would obtain a Gaussian distribution in logarithmic flux values and this is commonly referred as log-normal distribution. In such case, the flux distribution can be expressed as

$$f(x) = \frac{1}{\sigma\sqrt{2\pi}}\frac{1}{x}exp(\frac{-[log(x) - \mu]^2}{2\sigma^2}) \tag{1}$$

where, μ and σ are mean and standard deviation of log(x). Non-linearity expressed by a log-normal flux distributions suggests, the underlying process responsible for the flux variation to be a multiplicative one Uttley et al.(2005).

Log-normal flux distributions are often found in galactic and extragalactic sources, like X-ray binaries, gamma ray bursts and AGNs (Negoro & Mineshige 2002; Quilligan et al. 2002; Giebels & Degrange 2009). In case of AGNs the log-normal behaviour are observed on timescales ranging from minutes to days (Gaskell 2004); whereas, for X-ray binaries such behaviour are seen in sub-second time scales (Uttley et al. 2005). Among blazars, BL Lacertae is the first blazar in which log-normal variability is clearly detected in the X-ray regime (Giebels & Degrange 2009). Presently, such behaviour is seen across the electromagnetic spectrum for many BL Lac objects and FSRQs, e.g. PKS 2155-304 (Chevalier et

al. 2015), Mkn 421 (Sinha et al. 2016) and PKS 1510-089 (Kushwaha et al. 2016). In addition to the single log-normal distribution, double log-normal distribution in flux has also been found for some blazar sources at different energy bands (Kushwaha et al. 2016a; Shah et al. 2018).

The log-normal behaviour of these astrophysical sources are usually interpreted as processes happening at accretion disk. However, minute time-scale variability as seen in many blazars (Aharonian et al. 2007; Paliya et al. 2015) is difficult to originate from the disc (Narayan & Piran 2012), and strongly favours the variability to originate within the jet.

Besides the timing property another striking feature of blazar is that they show spectral variability. Various studies show that the X-ray spectrum of blazar exhibits mild curvature which can be fitted well with a log-parabola function. For a better understanding about the intrinsic curvature and its evolution, the physically motivated model is required.

In the first year of this project, we have gathered significant knowledge about their long term flux distributions and developed a numerical code to model the flux distribution. Then we have analyzed the flux and the photon spectral index light curves from the available, Monitor of All-sky X-ray Image ($MAXI$) data in the X-ray band to see whether the observational results are consistent with the Theoretical/Numerical results. In section-3, we present our model highlighting the plausible physical mechanism responsible for the obtained distributions.

In the second year of this project, we study the flux and the photon spectral index distributions of the blazar sources by using 16 years of the Rossi X-ray Timing Explorer ($RXTE$) archival data. Characterization of flux/index distribution and correlation study between the flux and photon index is described in Section-4.

In last year of this project, we performed a detailed analysis of the X-ray spectra of the blazar Mkn 421 using Swift-XRT observations taken between 2005 and 2020, to quantify the correlations between spectral parameters for different models.

3 Description of the work

We study the effect of a Gaussian perturbation in the acceleration timescale on the observed spectrum. To model the emission scenario of blazars, we consider here two-zones, one around the shock front where the acceleration of a mono energetic electron distribution take place and the next down stream where they lose most of their energy through radiative processes (Kirk et al. 1998; Sahayanathan 2008). We label the former zone as acceleration region(AR) and the latter as cooling region(CR). The kinetic equation describing evolution of the electrons in the AR region is given by (Kardashev 1962),

$$\frac{\partial n(\gamma, t)}{\partial t} + \frac{\partial}{\partial \gamma}\left[\left(\frac{\gamma}{\tau_a} - A\gamma^2\right) n(\gamma, t)\right] + \frac{n(\gamma, t)}{\tau_e} = Q\delta(\gamma - \gamma_0) \tag{2}$$

where, $A = \frac{1}{\gamma_{max}\tau_a}$ with γ_{max} being the maximum Lorentz factor that an electron can attain in the AR region, τ_a is the acceleration time scale of electrons in AR region and τ_e is the escape time scale of electrons in AR. The quantities τ_a and τ_e have been assumed independent of energy. The first term in the square bracket of equation (18) describes the acceleration at the rate τ_a^{-1}. The second term describes energy loss rate due to synchrotron/inverse Compton radiation. Mono energetic electrons with Lorentz factor γ_0 are injected into the acceleration region, get accelerated and escapes into the downstream region. For instance, in case of energy and time independent acceleration and escape timescales, equation (18) can be solved analytically and the corresponding steady state solution can then be obtained as

$$n_0(\gamma) = Q_0\tau_a\gamma^{-1-\frac{\tau_a}{\tau_e}}\left(1 - \frac{\gamma}{\gamma_{max}}\right)^{\frac{\tau_a}{\tau_e}-1}\left(\frac{1}{\gamma_0} - \frac{1}{\gamma_{max}}\right)^{-\frac{\tau_a}{\tau_e}} \tag{3}$$

Since several observations showed that there is a trend of log-normal behaviour in blazars at high energy regime, we choose to study the variation in the observed flux by perturbing the acceleration and escape time-scale of AR (τ_a and τ_e).

3.1 Gaussian perturbation on τ_a

We perturbed the steady state solution by introducing time variation in the acceleration time-scale (τ_a) of AR as, $\tau_a = \tau_{a0} + \Delta\tau_a$ and the corresponding variation in the particle number density can be conveniently expressed as $\bar{n}(\gamma) = \bar{n}_0(\gamma) + \Delta\bar{n}(\gamma)$, here, τ_{a0} is the mean value of the acceleration time-scale and $\bar{n}_0$ is the

steady state solution (equation ([3](#))) corresponding to $\tau_a = \tau_{a0}$. To further understand the flux variation in the particle distribution due to the perturbation on acceleration time-scale (τ_{a0}), we substitute the values of τ_a and $\bar{n}(\gamma)$ into the steady state solution of equation ([18](#)), hence the fractional variability of $\bar{n}(\gamma)$ can be expressed as,

$$\frac{\Delta \bar{n}(\gamma)}{\bar{n}(\gamma)} = f(\gamma)\frac{\Delta \tau_a}{\tau_a} + g(\gamma)\frac{\Delta \tau_a}{\tau_e} \tag{4}$$

where,

$$f(\gamma) = \left(\frac{1}{1 - \gamma/\gamma_{max}} \right) \tag{5}$$

$$g(\gamma) = \log \frac{\gamma_0(1 - \gamma/\gamma_{max})}{\gamma(1 - \gamma_0/\gamma_{max})} - \frac{\gamma/\gamma_{max}}{1 - \gamma/\gamma_{max}} + \frac{\gamma_0/\gamma_{max}}{1 - \gamma_0/\gamma_{max}} \tag{6}$$

This is evident from equation ([4](#)) that the variability in $\bar{n}(\gamma)$ is a linear combination of Gaussian and log-normal terms and the corresponding relative amplitudes of these terms are decided by the functions $f(\gamma)$ and $g(\gamma)$. For the case $\gamma_{max} \to \infty$, the log-normal term dominates when $\gamma \gg \gamma_0 \exp(\tau_e/\tau_a)$.

To verify the deviation of $n(\gamma, t)$ from a Gaussian, we simulate its time series for 5000 points by solving equation ([18](#)) numerically using finite difference scheme. The values of γ_0 and γ_{max} are kept fixed at 10 and 10^5 respectively. The generated time series are then investigated for various statistical properties.

In Figure 1(a), we plot the skewness of the accelerated electron distribution (κ_n) as a function of σ_{τ_a}/τ_a for different values of γ. We see that while for very low values γ ($\gamma < 30$), the distribution is slightly negatively skewed, the distribution becomes highly tailed for increasing values of γ. We thus check the consistency of the distributions with a lognormal by computing the skewness of the logarithm of the fluxes (Figure 1(c)), which, for large values of γ, is found to be consistent with zero, hence reflecting lognormal distribution. As a further confirmation, we fit the normalised histograms of the fluxes with normal and lognormal functions and compare the results using a χ^2 test. The lognormal distribution with $\chi^2_{red} \approx 1.1$ is significantly favoured at high energies (Fig 2(a)).

3.2   Gaussian perturbation on τ_{ea}

We repeat the same analysis as above, but we now introduce small time variations in the escape time scale in the AR as, $\tau_e = \tau_{e0} + \Delta\tau_e$ and the corresponding change in the electron number density as $\tilde{n}(\gamma) = \tilde{n}_0(\gamma) + \Delta\tilde{n}(\gamma)$ where, $\tilde{n}_0$ is the steady state solution (equation ([3](#))) corresponding to $\tau_e = \tau_{e0}$. Following the similar procedure as is described in the previous section, the fractional variability in $\tilde{n}(\gamma)$ can then be obtained as,

$$\frac{\Delta \tilde{n}}{\tilde{n}} = \tau_a \frac{\Delta \tau_e}{\tau_e^2} \log \frac{\gamma(1 - \gamma_0/\gamma_{max})}{\gamma_0(1 - \gamma/\gamma_{max})} \tag{7}$$

Thus, the particle distribution should be a right skewed one, but not a lognormal. We plot in Figure 1(b) and 1(d) the skewness of n(γ) and log(n(γ)) as a function of σ_{τ_e}/τ_e for different values of γ. The distribution is highly tailed for increasing values of γ. However, the distribution is not lognormal, as we see that the skewness of the logarithm of the fluxes (Figure 1(d)) becomes negative. In Figure 2(b), we show the fitted histograms of the fluxes are fitted with normal ($\chi^2_{red} \approx 6.7$) and lognormal ($\chi^2_{red} \approx 3.7$) functions, a large reduced-χ^2 is returned for both the distributions suggest both of these functions cannot represent the given distribution.

3.3   Study of Observation

we study the X-ray observations of the blazar Mkn 421 by $MAXI$[1] satellite. Analysis of 9 years (Matsuoka et al. 2009) of continuous data with 10 days binning showed that the distribution is clearly preferred to be a lognormal ($\chi^2_{red} \approx 1.2$) over a Gaussian ($\chi^2_{red} \approx 6.0$) (Figure 3(b)), the spectral index is normally distributed with $\chi^2_{red} \approx 0.81$ for 10 dof, mean $m_p = 2.1 \pm 0.022$ and standard deviation $\sigma_p = 0.31 \pm 0.096$ (Figure 3(a)). This suggests that the plausible physical process responsible for the observed flux variation is associated with the fluctuations in the particle acceleration rate. A comparison of Figure 1(a) with the value, $\sigma_{\tau_a}/\tau_a = \sigma_p/m_p \approx 0.148 \pm 0.046$ and the observed skewness of $\kappa = 1.27 \pm 0.24$ suggests the emission to originate from electrons with γ range $\sim 10^2 - 10^3$. However, this estimate of γ is significantly lower than the electron energies obtained through the broadband spectral modelling of the source using

---

[1] http://maxi.riken.jp/top/lc.html

synchrotron and inverse Compton emission mechanisms (Sinha et al. 2016). This discrepancy in the estimation of γ can be associated with the low value of the injection lorentz factor γ_0 which is fixed at 10 for the present study. However if we take higher γ_0, the result can be consistent with the ones obtained through spectral modelling.

4 RXTE archive and source selection

The Rossi X-ray Timing Explorer ($RXTE^2$) satellite provides 16 years light curves of AGNs including Seyfert 1s, Seyfert 2s, and Blazars during the period 1996 January to 2012 January. It provides light curves in the energy range 2-10 keV, 2-4 keV, 4-7 keV and 7-10 keV. The data sampling in the light curves is uneven since different viewing schemes were proposed for each object at various times and for various scientific goals. However, despite the time gaps in the light curves, 16 years long light curves provides a large data set, which are suitable to study the variable properties.

In our study, two BL Lacs were chosen such that the flux and index light curves in the energy range of 2–10 keV, have number of data points more than 90. Further, to select the light curves with good statistics, we define the significance fraction for the light curve as,

$$R = \frac{\overline{\sigma_{err}^2}}{\sigma^2} \tag{8}$$

where $\overline{\sigma_{err}^2}$ is the mean square error of flux/index distribution and σ^2 is the variance of flux/index distribution. From the selected blazars, only those sources were considered for further analysis which has $R < 0.2$ in both the flux and index light curves. However, the above mentioned condition was not satisfied for the light curves which were downloaded from the $RXTE$ website. Therefore, we binned the light curves by combining the data point in the flux/index light curves from 2 days to a maximum of 10 days. Then, after applying these conditions that is, number of points in the light curve ≥ 90 and $R < 0.2$, we have two BL Lacs viz. Mkn 501, Mkn 421. These BL Lac objects viz. Mkn 501 and Mkn 421 are located at a redshift of 0.033 and 0.031 respectively, and are very well known high synchrotron peaked BL Lac (HBL) objects, with the low energy SED component peaking at frequency $\nu_p > 10^{15.3}$ Hz. The selected light curves are then investigated for various statistical properties such as, Anderson-Darling (AD) test statistic and fitting histograms. The length of light curves and the R values of Mkn 501 and Mkn 421 are given in Table-1.

4.1 AD test

Anderson-Darling (AD) test is a statistical test of whether a given sample of data is drawn from a given probability distribution (here, normal distribution). The AD test calculates the null hypothesis probability value (p–value) such that p–value > 0.01 indicates the normality of the sample and p–value < 0.01 indicates the deviation from the normality. The AD test results for Mkn 501 and Mkn 421 show that p–values for flux in linear-scale and log-scale are much smaller than 0.01, which indicates that the flux distribution will be neither normal nor log-normal. Moreover, the p–value of index distribution also suggests a non-normal distribution of index in Mkn 501 and Mkn 421. The AD test results are reported in Table-2.

4.2 Histogram of flux and index

Histogram fitting is also an useful tool to understand the nature of the distribution. We constructed the normalized histograms of logarithm of flux and index in normal-scale with equal number of flux/index points in each bin. In case of Mkn 501 and Mkn 421, the flux and index histograms show a double-peaked structure. Also, the AD test results of these two BL Lacs show that the flux distribution is neither Gaussian nor log-normal, and the index distribution is not Gaussian. We therefore, analyzed the distribution of these two sources with double PDF, given by

$$d(x) = \frac{a}{\sqrt{2\pi\sigma_1^2}} e^{\frac{-(x-\mu_1)^2}{2\sigma_1^2}} + \frac{(1-a)}{\sqrt{2\pi\sigma_2^2}} e^{\frac{-(x-\mu_2)^2}{2\sigma_2^2}} \tag{9}$$

where, a is the normalization fraction, μ_1 and μ_2 are the centroids of the distribution with widths σ_1 and σ_2, respectively. The fit of flux histogram in log-scale and index histogram in linear-scale with equation

---

[2] https://cass.ucsd.edu/~rxteagn/

Table 1: Light curve significance fraction R values for the unbinned/binned flux and index light curves. Col:- 1: Selected blazars satisfying the conditions R<0.2 and length of binned flux/index light curve $\geq$ 90, 2: Number of data points in the distributions, 3: R-value for index light curve, and 4: R-value for the flux light curve.

Blazar name	Number of data points	R_Γ	R_{Flux}
Mkn 501	496 (unbinned)	0.05	1.0×10^{-4}
	188 (2-days binned)	0.06	1.0×10^{-4}
Mkn 421	1182 (unbinned)	0.75	6.8×10^{-5}
	93 (10-days binned)	0.17	9.6×10^{-6}

Table 2: AD test results for the flux/index distribution of three selected blazars viz. Mkn 501 and Mkn 421 Col:- 1: Selected blazars satisfying the conditions R<0.2 and length of binned flux/index light curve $\geq$ 90, 2: Number of data points in the distributions, 3,4: AD statistics for Flux and Logarithm of flux distribution, and 5: AD statistics for index distribution.

Blazar name	Number of data points	Normal (Flux) AD(p–value)	Log-normal (Flux) AD(p–value)	Normal (Spectral index) AD(p–value)
Mkn 501	188 (2-days binned)	15.89 ($< 2.2 \times 10^{-16}$)	2.78 (4.96×10^{-7})	1.24 (3.0×10^{-3})
Mkn 421	93 (10-days binned)	2.29 (7.44×10^{-6})	1.27 (2.5×10^{-3})	1.09 (7.0×10^{-3})

(10) will result in the double log-normal fit of the flux distribution and double normal fit of the index distribution. The best fit parameter values of fitting the double distribution flux/index histograms are given in Table-3 and corresponding plots are shown in figures 4 and 5. The double log-normal fit to flux histograms of Mkn 501 and Mkn 421 gave a χ^2/dof of 38.28/33 and 11.85/15 respectively, while as the other double distribution functions, such as combination of log-normal and Gaussian gave a χ^2/dof of 38.38/33 for Mkn 501 and 12.75/15 for Mkn 421. Combination of Gaussian and log-normal gave a χ^2/dof of 50.36/33 for Mkn 501 and 14.10/15 for Mkn 421, while a double Gaussian fit gave a χ^2/dof of 41.58/33 for Mkn 501 and 14.70/15 for Mkn 421. These reduced χ^2 values suggest that the double log-normal fit and lognormal-Gaussian fit to the flux histograms of two BL Lacs are equally good. Further, we found that the photon index distribution in both Mkn 501 and Mkn 421 are fitted with the double Gaussian distribution function with χ^2/dof of 39.1/34 and 16.94/14 respectively. The best fit parameter values of the double distribution are reported in Table-3.

4.3 Correlation study

We, further performed the Spearman's rank correlation study between flux and index. The Spearmans rank correlation coefficient is the non-parametric statistical measure used to study the strength of association between the two ranked variables. The correlation parameters i.e., Spearman's rank correlation coefficient (r_s), its chance correlation probability (P) and the correlation slope (A) show a significant negative correlation between the flux and index for all the selected blazar sources, which is the usual trend blazars show across the electro-magnetic spectrum (Pandey et al. 2017; Brown & Adams 2011). The correlation parameter values are summarized in Table-4. In the correlation plots (left top panel in Figs 4 and 5), gray bands represent the 1- error on the centroids of the logarithm of flux and index distributions (Figs 4 and 5). In the bottom panel of Fig. 5, the error on higher index centroid is large, so a single vertical line is shown instead of a gray band.

Table 3: Best fit parameter values of the double PDF (equation 10) fitted to the logarithm of flux and index histograms. Col:- 2: Histogram obtained from the logarithm of flux and linear index distribution, 3–6: Best fit values of μ_1, σ_1, μ_2 and σ_2, 7: Normalization fraction, 8: Degrees of freedom and 9: Reduced χ^2.

Blazar	Histogram	μ_1	σ_1	μ_2	σ_2	a	dof	χ^2/dof
Mkn 501	log10(Flux)	-9.62±0.04	0.10±0.03	-10.02±0.02	0.14±0.02	0.83±0.06	33	1.16
	Index	1.74±0.03	0.09±0.02	2.19±0.02	0.15±0.01	0.83	34	1.15
Mkn 421	log10(Flux)	-9.36±0.05	0.26±0.05	-10.10±0.08	0.29±0.08	0.3	15	0.79
	Index	2.54±0.05	0.21±0.04	3.09±0.48	0.51±0.31	0.3	14	1.21

Table 4: Spearman Correlation results obtained by comparing flux and index distribution of three selected blazars. Col:- 1: Selected blazar sources 2: Spearman's rank correlation coefficient (r_s), 3: Probability chances for correlation (P) and 4: Slope of the best fitted line to correlation plots (A).

Blazar name	r_s	P	A
Mkn 501	-0.65	2.96×10^{-24}	-0.94±0.06
Mkn 421	-0.86	7.25×10^{-29}	-1.21±0.07

4.4 Conclusions

The correlation study between the flux and index of the selected blazars, shows a significant negative correlation, which is expected. Moreover, when the index distribution is double Gaussian, the flux is also preferred to be double distributed. Using the interpretation of our first paper (Sinha et al. 2018) (the work of the first paper during the year 2017-2018, is also mentioned in section-3 here), the double Gaussian distribution in the index would preferably indicate double log-normal distribution in flux. In the paper, we showed that Gaussian distribution in the index can be initiated through linear fluctuations in the particle acceleration rate and hence, the log-normal flux distribution may carry information regarding the acceleration processes in the blazar jets. However, studying the flux and index distributions over a long timescale at different wavebands, would be important to probe the information of variability more in detail.

5 Spectral study of Mkn 421

Mkn 421 is the nearest (z = 0.031) HBL type object, with the peak frequency of the low-energy component beyond $10^{15.3}$ Hz. It was also the first blazar observed at TeV energies using the Whipple telescope (Punch et al. 1992), and thus classified it as a TeV blazar. Several X-ray observations suggest that the X-ray spectrum of Mkn 421 exhibits a well-marked curvature during both flaring and quiescent states and consequently the spectrum cannot be fitted by the simple power-law model. The observed curved spectrum is found to be well fitted by the log-parabola function (Wierzcholska & Wagner 2016; Gaur et al. 2017). However, Hota et al. 2021 had shown with the approach of spectral parameter correlations that curved spectrum can be interpreted as an outcome of energy dependent acceleration and diffusion of the particles.

In this study, we present for the first time, the spectral study of Mkn 421 using an entire collection of Swift-XRT data available during the period April 2005 to April 2020. NASAs HEASARC interface [3] provides the Swift-XRT data in the 0.310 keV band. We fit each spectrum with different particle energy distribution models viz. log-parabola model, power-law particle distribution with maximum electron energy, energy-dependent diffusion (EDD), and energy-dependent acceleration (EDA) models, and the corresponding results are discussed. We perform a correlation study between the best fit model parameters and compare them with the ones obtained from the log-parabola spectral fit. Hota et al. 2021, used these models and showed that the correlations between the spectral parameters for a single short-term flare with a duration $\approx$ 400 ksec can be used to constraint different models and provide an assessment of the underlying physical quantities. The motivation of this work is to test whether the correlation results from the long-term observations are consistent with the one obtained from short-term flare (Hota et al. 2021).
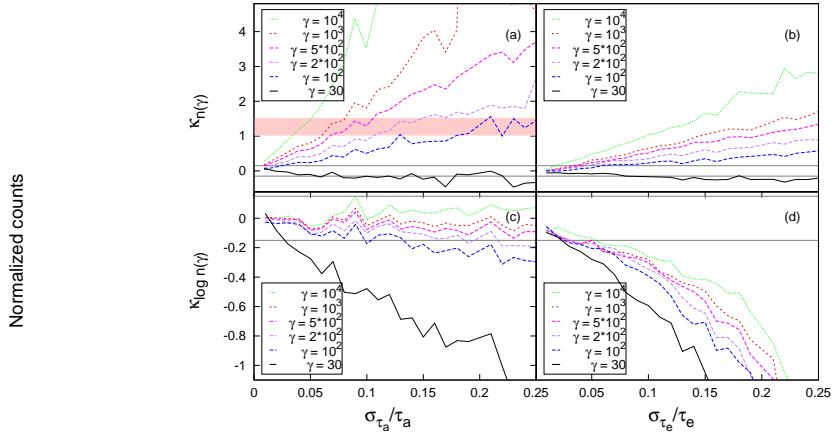
---

[3]https://heasarc.gsfc.nasa.gov/

Figure 1: Skewness (κ) of the simulated particle distribution as a function of σ_{τ_a}/τ_a and σ_{τ_e}/τ_e is shown in (a) and (b), whereas the skewness of the logarithm of the distribution as a function of σ_{τ_a}/τ_a and σ_{τ_e}/τ_e is shown in (c) and (d). The solid line corresponds to electron with Lorentz factor $\gamma = 30$ (black), dashed line to $\gamma = 10^2$ (blue), dashed line to $\gamma = 2 * 10^2$ (purple), dashed line to $\gamma = 5 * 10^2$ (magenta), short dashed line to $\gamma = 10^3$ (red) and dotted line $\gamma = 10^4$ (green). The grey lines show the 3-σ ($3\sqrt{15/N}$) error range. The pink band shows the 1-σ error range for the observed value for Mkn421 (sec-3.3)
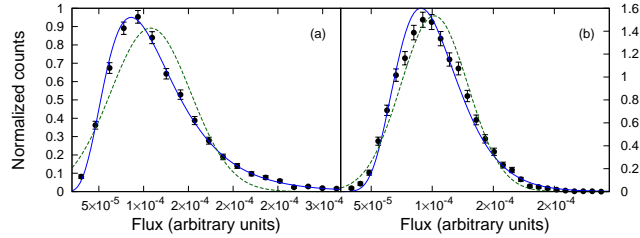
Figure 2: Fig 2(a) and 2(b) represent the histograms of the simulated particle number density for $\sigma_{\tau_a}/\tau_a = 0.1$, $\sigma_{\tau_e}/\tau_e = 0.1$ and $\gamma = 10^3$. The dashed green line represents the best fit Gaussian and the solid blue line represents the best fit log-normal functions.
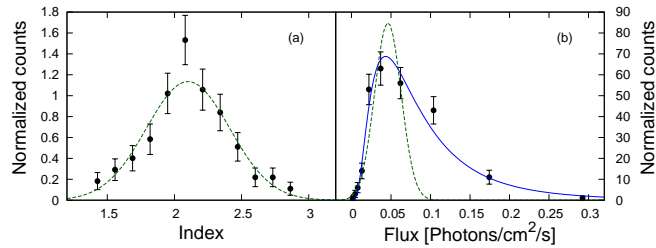

Figure 3: Histograms of the 10 day binned X-ray (a) spectral index at 2-10 keV and (b) 2-20 keV flux of Mkn 421 spanning over 9 years.
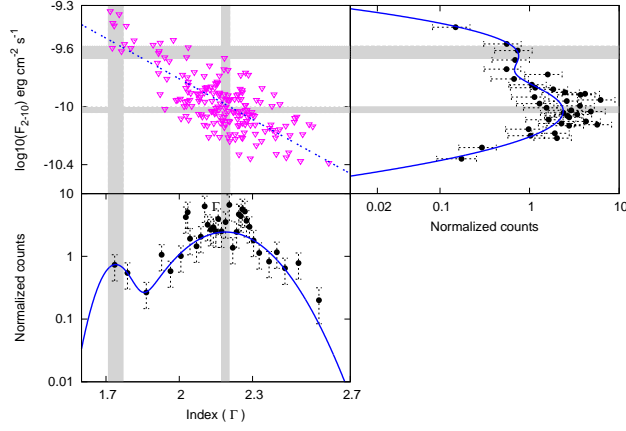
Figure 4: Multi-plot for the characterization of flux/index distribution of Mkn 501. Top panel left is the logarithm of flux vs index scatter plot along with the best fit line (dotted line). Top panel right is the histogram of logarithm of flux distribution. Bottom panel is the histogram of index distribution. The solid curve in the top panel right and bottom panel indicates the best fitted double PDF (equation 10). The vertical and horizontal gray bands indicate the 1-σ error range on the centroids ($\mu1$, $\mu2$) of the double PDF (equation 10) fitted to the index distribution and logarithm of flux distribution respectively.
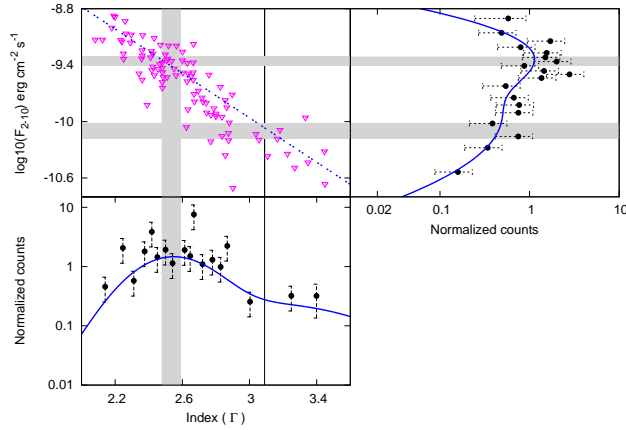

Figure 5: Multi-plot for the characterization of flux/index distribution of Mkn 421. The three panels in this plot are same as described in Fig. 4. A single vertical line represents the centroid value of the higher index distribution (Section 4.3).

5.1 Spectral analysis

The X-ray spectrum of Mkn 421 is known to be produced by the non-thermal relativistic electrons undergoing synchrotron emission. Hence we model the non-thermal X-ray emission from Mkn 421 by assuming that the emission originates from a spherical region of radius, R. The emission region is assumed to be filled with tangled magnetic field, B and relativistic isotropic electron distribution, n(γ) which undergoes synchrotron loss. The synchrotron emissivity due to a relativistic electron distribution n(γ) can be estimated by using the equation

$$J_{\text{syn}}(\epsilon') = \frac{1}{4\pi} \int P_{\text{syn}}(\gamma, \epsilon')\, n(\gamma)\, d\gamma \tag{10}$$

here, $P_{\text{syn}}(\gamma, \epsilon')$[4] is the pitch angle averaged synchrotron power emitted by single particle and can be obtained using the equation (Rybicki & Lightman 1986).

$$P_{\text{syn}}(\gamma, \epsilon') = \frac{\sqrt{3}\pi e^3 B}{4 m_e c^2} f\left(\frac{\epsilon'}{\epsilon_c}\right) \tag{11}$$

where $\epsilon_c = \frac{3 h e \gamma^2 B}{16 m_e c}$ and $f\left(\frac{\epsilon'}{\epsilon_c}\right)$ is the synchrotron power function defined as (Rybicki & Lightman 1986).

$$f(x) = x \int_x^\infty K_{5/3}(\psi)\, d\psi \tag{12}$$

with $K_{5/3}$ being the modified Bessel function of order 5/3. Using the single particle synchrotron power (Equation 11), and substituting $\xi = \gamma\sqrt{C}$, where $C = \frac{\delta}{1+z}\frac{3heB}{16m_e c}$ with z being the redshift of source and δ as jet Doppler factor, the synchrotron emissivity in the observed frame can be obtained as

$$J_{\text{syn}}\left(\frac{1+z}{\delta}\epsilon\right) = A \int_{\xi_{min}}^{\xi_{max}} f(\epsilon/\xi^2) n(\xi) d\xi \tag{13}$$

where $A = \frac{\sqrt{3}\pi e^3 B}{16 m_e c^2 \sqrt{C}}$. Finally, the synchrotron flux received by the observer at energy ϵ will be given by Begelman et al. 1984,

$$F_{\text{syn}}(\epsilon) = \frac{\delta^3(1+z)}{d_L^2} V J_{\text{syn}}\left(\frac{1+z}{\delta}\epsilon\right) = \frac{\delta^3(1+z)}{d_L^2} V A \int_{\xi_{min}}^{\xi_{max}} f(\epsilon/\xi^2) n(\xi) d\xi \tag{14}$$

where, d_L is the luminosity distance, and V is the volume of the emission region. This SYNchrotron CONVolution equation including single-particle emissivity and particle number density is solved numerically and is used as a local convolution model *(synconv ⊗ n(ξ))* in XSPEC (Version 12.11.0) software package 1996ASPC..101...17A. In the model, the XSPEC "energy" variable is represented as $\xi = \sqrt{C}\gamma$ such that the corresponding observed photon energy is $\epsilon = \xi^2$ 2021MNRAS.tmp.2632H. The *(synconv ⊗ n(ξ))* model outputs the synchrotron spectrum for a system with particle density, $n(\xi)$ as an input to the model. In this work, we have used log-parabola function and energy dependent physical models as input particle density to the *(synconv ⊗ n(ξ))* model. We performed the spectral fit for each of the resultant grouped spectra obtained in the energy-range 0.3-10 keV, while we added 3% systematics to the data in order to reduce emission model related uncertainties. During the fit, the neutral hydrogen column density, $N_H = 1.92 \times 10^{20} cm^{-2}$ was kept froze, the N_H value is obtained in the LAB survey (Kalberla et al. 2005).

5.1.1 Log-parabola model

Firstly, we consider the case when the underlying particle density is described by the log-parabola function, and is defined by,

$$n(\gamma)d\gamma = K(\gamma/\gamma_r)^{-\alpha-\beta\log(\gamma/\gamma_r)}d\gamma \tag{15}$$

Here, α is the particle spectral index at the reference energy, $E_r = \gamma_r mc^2$, β and K are the curvature parameter and the normalization, respectively. The synchrotron convoluted equation involves ξ parameter instead of γ, therefore, replacing γ by $\xi/\sqrt{C}$, the log-parabola function takes the form as

$$n(\xi) = K(\xi/\xi_r)^{-\alpha-\beta\log(\xi/\xi_r)} \tag{16}$$

---

[4]In this paper, the ′ indicates that the physical quantity is estimated in the emission region frame.

During the spectral fit with $synconv \otimes n(\xi)$ model (Equation 14), $\xi_r{}^2$ was fixed at 1 keV, therefore the spectrum is determined by the three free parameters, viz. α, β, and norm N. From Equations 14 and 16, N can be obtained as

$$N = \frac{\delta^3(1+z)}{d_L^2} V A K \qquad (17)$$

The obtained model is then fitted to each spectrum of the XRT observations. To assess the significance of any correlation or anticorrelation between the best fit parameters, we used Monte Carlo simulation technique. For each data point and its corresponding error in the time series, we simulated 10,000 random datasets by considering the underlying normal distribution of observed data points. The Spearman's rank correlation coefficient r_s and null hypothesis probability P_s were calculated using the simulated datasets. The correlation results between best fit parameters and flux are shown in Table 5, where the top panel corresponds to the log-parabola model. The correlation plots between the log-parabola model fit parameters and the 0.3-10 keV flux ($F_{0.3-10keV}$), are shown in Fig. 7. Analogous to the previous results, a strong anticorrelation between α and $F_{0.3-10keV}$ with r_s (P_s) as -0.81 ± 0.005 (4.67×10^{-229}) is observed, which implies a harder when brighter behavior in the spectrum (Massaro et al. 2004, 2008). However, there is no correlation between β and $F_{0.3-10keV}$ with r_s (P_s) as 0.04 ± 0.02 (0.27). In addition, a weak anticorrelation is observed between α and β with r_s (P_s) as -0.21 ± 0.02 (7.68×10^{-9}), such negative trend between α and β was seen by Goswami et al. 2018 in some short-term flares. On the other hand, no correlation was seen between α and β during January 2013 – June 2014 (Kapanadze et al. 2016, 2017). Furthermore, we obtained a nearly moderate anticorrelation between α and N with r_s (P_s) as -0.41 ± 0.008 (1.78×10^{-39}), and a mild positive correlation between β and N with r_s (P_s) as 0.15 ± 0.02 (2.37×10^{-5}). The log-parabola model is the limited version of more general physical model under some specific scenarios, as described in sections 3.3.1 & 3.3.2. In the following subsection, we will discuss the physical models and their capability of reproducing the observed spectrum.

5.2 Power-law particle distribution with maximum electron energy

We refit the spectra by considering the shape of particle density as power-law model with maximum electron energy. In this case, we consider the particle acceleration mechanism and radiative losses. The spectral curvature in the power-law particle distribution is obtained due to fast decay of emitting particles near the maximum available particle energy $\gamma_{max}mc^2$, where γ_{max} is the maximum Lorentz factor that an electron can attain before it loses energy. Here we consider that the particles are accelerated through Fermi acceleration process near the shock front and lose energy by emitting radiation through the synchrotron process. The steady-state evolution of electrons in such a region is governed by Kardashev et al. 1962,

$$\frac{\partial}{\partial \gamma}\left[\left(\frac{\gamma}{t_{acc}} - \Lambda_a \gamma^2\right) n_a\right] + \frac{n_a}{t_{esc}} = Q_o \delta(\gamma - \gamma_0) \qquad (18)$$

where $\Lambda_a = \frac{1}{\gamma_{max}t_{acc}}$, t_{acc} and t_{esc} are the acceleration and escape time scales of electrons, $\Lambda_a\gamma^2$ describes the radiative energy loss rate. If we consider the case of t_{acc} and t_{esc} being energy independent, such that their ratio is defined as,

$$\frac{t_{acc}}{t_{esc}} = p - 1 \qquad (19)$$

where p is the particle spectral index, then the steady-state solution of Equation 18 can be obtained as (Kirk et al. 1998),

$$n(\gamma)d\gamma = K\gamma^{-p}\left(1 - \frac{\gamma}{\gamma_{max}}\right)^{(p-2)}d\gamma \qquad (20)$$

where $K = Q_0 t_a \gamma_0^{p-1} C^{p/2}$, here Q_0 is mono-energetic injection at minimum energy, γ_0. Again the $synconv \otimes n(\xi)$ model (Equation 14) used for spectral fit contains ξ instead of γ, therefore replacing γ by $\xi/\sqrt{C}$ in 20, we have

$$n(\xi) = K\xi^{-p}\left(1 - \frac{\xi}{\xi_{max}}\right)^{(p-2)} \qquad (21)$$

where $\xi_{max} = \gamma_{max}\sqrt{C}$. We performed the fit with the convolved spectral model, $synconv \otimes n(\xi)$; where $n(\xi)$ is given by Equation 21 (hereafter ξ_{max} model), for all the available $Swift$-XRT observations. The fit

is carried with three parameters viz. norm N, ξ_{max} and p. In this model, the number of free parameters are same as the log-parabola model. Here N is defined as

$$N = \frac{\delta^3(1+z)}{d_L^2} V \, A Q_0 t_{acc} \gamma_0^{p-1} C^{p/2} \tag{22}$$

The model provides a reasonable fit to the X-ray spectrum in the energy range 0.3–10 keV, and the reduced-χ^2 values obtained from the ξ_{max} model are equally good as those obtained from the log-parabola model. The difference of the reduced-χ^2 values for the log-parabola and the ξ_{max} model, vs. reduced-χ^2 of the log-parabola model is shown in Fig. 6(a). The correlation results between the ξ_{max} model parameters are reported in the second rows of Table 5, and the plots are shown in Fig. 8. A strong anticorrelation is observed between p and flux, $F_{0.3-10keV}$ with r_s (P_s) as -0.80 ± 0.007 (1.92×10^{-209}), while no correlation is obtained between ξ_{max} and $F_{0.3-10keV}$ with r_s (P_s) as -0.03 ± 0.02 (0.44). A weak anticorrelation is obtained between p and N with r_s (P_s) as -0.28 ± 0.009 (6.31×10^{-19}), and ξ_{max} vs. N with r_s (P_s) as -0.15 ± 0.02 (2.28×10^{-4}). The weak correlation between ξ_{max} and N can be expected as the functional form of N (Equation 22) is independent of ξ_{max}. However, the weak anticorrelation obtained between p and N contradicts with the functional form of N (as $\log N \propto p$ see Equation 22). Moreover, a weak positive correlation is observed between ξ_{max} and p with r_s (P_s) as 0.20 ± 0.02 (4.94×10^{-7}). In the Fermi acceleration scenario, the ξ_{max} is decided by the acceleration rate and radiative loss such that $\xi_{max} \propto \frac{1}{t_{acc}B^{3/2}}$ and $p \propto t_{acc}$. Therefore, an anticorrelation is expected between ξ_{max} and p, which disputes with the weak positive correlation observed between ξ_{max} and p. These disputes suggest that the PL with maximum electron energy model is not suitable for reproducing the observed synchrotron spectrum. However, the model can be consistent with the observations if we consider the following conditions. The acceleration time-scale varies with the magnetic field such as $t_{acc} \propto B^{-n}$ or $B \propto (p-1)^{-\frac{1}{n}}$. Consequently, $\xi_{max} \propto B^{n-3/2} \propto (p-1)^{-(n-3/2)/n}$. Therefore, a positive correlation is expected between ξ_{max} and p if $n < \frac{3}{2}$ and linear correlation is expected if $n \sim \frac{3}{4}$.

5.3 Energy dependent model:

Alternatively, the physical models with the energy dependent escape time-scale [$t_{esc}(\gamma)$] or the energy dependent acceleration time-scale [$t_{acc}(\gamma)$], can also explain the spectral curvature. Again we consider that the electrons gain energy mainly by crossing the shock front such that t_{acc} is determined by the time-scale at which particles cycle across the shock and these accelerated electrons diffuse away from shock region at a rate $1/t_{esc}$, move to the downstream region and finally lose energy by emitting the synchrotron radiations.

5.3.1 t_{esc} is energy dependent (EDD model)

In the jet environment, the diffusion occurs in the region filled with magnetic field, which can make the escape time scale dependent on the gyration radius of electron. This inturn can make escape time scale energy dependent. Here we parameterize the energy-dependent as

$$t_{esc} = t_{esc,R} \left(\frac{\gamma}{\gamma_R} \right)^{-\kappa} \tag{23}$$

where, $t_{esc,R}$ corresponds to t_{esc} when the electron energy is $\gamma_R mc^2$, and κ decides on the energy dependence of the escape of electrons. Here, t_{esc} can not be larger than the free streaming value, $t_{esc,R}$, and this set limits on γ to $\gamma < \gamma_R$. Consequently for $\gamma_0 < \gamma$ and if we neglect the synchrotron energy loss, the electron energy distribution with the energy dependence of t_{esc} will take the form 2021MN-RAS.tmp.2632H,

$$n(\xi) = Q_o t_{acc} \sqrt{C} \xi^{-1} \exp\left[-\frac{\eta_R}{\kappa} \left(\left(\frac{\xi}{\xi_R} \right)^\kappa - \left(\frac{\xi_0}{\xi_R} \right)^\kappa \right) \right] \tag{24}$$

Here, $\eta_R \equiv t_{acc}/t_{esc,R}$, $\xi_R = \sqrt{C}\gamma_R$ and $\xi_0 = \sqrt{C}\gamma_0$. In case of $\kappa << 1$, the particle distribution will be represented by a log-parabola distribution such that, $n(\xi) \propto (\xi/\xi_R)^{-\eta_R-1-\eta_R\kappa log(\xi/\xi_R)}$, while for the case $\xi \to 0$, the solution will be identical to the one given in Equation 21 for $p = 1 + \eta_R$ and $\gamma << \gamma_{max}$ i.e., the case when escape time-scale will be energy independent or equal to the free streaming value, $t_{esc,R}$.

The details of these assumptions are given in 2021MNRAS.tmp.2632H. During the spectral fitting, there is degeneracy in the parameters associated with Equation 24. Therefore, we remove the degenerate parameters and use the modified Equation as follows,

$$n(\xi) = K\sqrt{C}\xi^{-1}\exp\left[-\frac{\psi}{\kappa}\,\xi^\kappa\right] \tag{25}$$

where

$$\psi = \eta_R\left(\frac{1}{C\gamma_R^2}\right)^{\kappa/2} = \frac{\eta_R}{\xi_R^\kappa} \tag{26}$$

and the normalization K is given below

$$K = Q_0\,t_{acc}\exp\left[\frac{\eta_R}{\kappa}\,\left(\frac{\gamma_0}{\gamma_R}\right)^\kappa\right] \tag{27}$$

The free parameters of $synconv \otimes n(\xi)$ model in this case are norm N, ψ and κ, where N is defined as

$$N = \frac{\delta^3(1+z)}{d_L^2}VAK\sqrt{C} \tag{28}$$

While carrying the spectral fit of the available Swift-XRT observations of Mkn 421 with $synconv \otimes n(\xi)$ model, $n(\xi)$ is given by equation 25. In Fig. 6(b), we have plotted the difference of the reduced-χ^2 values for the log-parabola and the energy-dependent t_{esc} model vs. reduced-χ^2 values of the log-parabola model. The figure shows that both the log-parabola and the EDD model fit the X-ray spectrum well. The Spearman-rank correlation results between the EDD model fit parameters are presented in the third rows of Table 5, and the correlation plots are shown in Fig. 9. A low positive correlation is observed between κ and flux, $F_{0.3-10keV}$ with r_s (P_s) and 0.32 ± 0.02 (3.30×10^{-19}), while a strong negative correlation is observed between ψ and flux, $F_{0.3-10keV}$ with r_s (P_s) values as -0.76 ± 0.008 (1.01×10^{-180}) respectively. equation 26 suggests an anti-correlation between $\log_{10}\psi$ and κ, which is seen in scatter plot between $\log_{10}\psi$ and κ (see Fig. 9 (a)), the Spearman rank correlation method shows a moderate anticorrelation with r_s (P_s) as $\sim -0.51 \pm 0.01$ (3.65×10^{-51}). To obtain the value of ξ_R, we express equation 26 as

$$\log_{10}\psi = \log_{10}\eta_R - \kappa\log_{10}\xi_R \tag{29}$$

The χ^2-fit of equation 29 to the scatter plot resulted in slope, $\log_{10}\xi_R = 0.52$ and the y-intercept, $\log_{10}\eta = 0.49$, which implies that $\xi_R \sim 3.31$ keV and $\eta_R \sim 3.09$. Therefore, the photon energy corresponding to γ_R will be $\xi_R^2 \sim 10.96$ keV which is slightly higher than the energy range, 0.3–10 keV considered for the spectral fitting. Furthermore, the correlation between the best-fit parameters κ and N can be used to estimate the energy of the electron at which they are injected. The normalization in Equation 28 can be written as

$$\log N = \frac{\eta_R}{\kappa}\,A^\kappa + B \tag{30}$$

We fit the plot shown in Fig. 9(b) with the above equation which results A = 0.045, B = 4.33, and η_R = 3.09, implies the value of $\gamma_0 \sim 0.045\,\gamma_R$, which is significantly smaller than γ_R.

5.3.2 t_{acc} is energy dependent (EDA model)

Here, we consider a scenario in which radiative loss due to synchrotron emission happens in the vicinity of the shock front instead of particles losing energy in the downstream flow as in the EDD model. In this case, we assume that the magnetohydrodynamic turbulence in jet flow makes t_{acc} to be energy-dependent while t_{esc} to be energy independent such that the energy dependence of t_{acc} is defined by $t_{acc} = t_{acc,R}\left(\frac{\gamma}{\gamma_R}\right)^\kappa$, here κ decides on the energy dependence of t_{acc}. Using Equation 18, the steady-state solution of kinetic equation describing the particle distribution when t_{acc} is energy dependent and ignoring the synchrotron energy loss.

$$n(\xi) = Q_0 t_{acc,R}\sqrt{C}\xi_R^{-\kappa}\xi^{\kappa-1}\exp\left[-\frac{\eta_R}{\kappa}\left(\left(\frac{\xi}{\xi_R}\right)^\kappa - \left(\frac{\xi_0}{\xi_R}\right)^\kappa\right)\right] \tag{31}$$

Here, $\eta_R \equiv t_{acc,R}/t_{esc}$, $\xi_R = \sqrt{C}\gamma_R$ and $\xi_0 = \sqrt{C}\gamma_0$. For $\kappa << 1$, the particle distribution will again represent a log-parabola distribution such that, $n(\xi) \propto (\xi/\xi_R)^{-\eta_R+\kappa-1-\eta_R\kappa log(\xi/\xi_R)}$, and for the case

$\kappa \to 0$ and $\gamma << \gamma_{max}$, the solution is similar to Equation 21. The particle energy distribution will reduce to the below form, when we ignore the degeneracy in the parameters in Equation 31, as given by

$$n(\xi) = K\sqrt{C}\xi^{\kappa-1}\exp\left[-\frac{\psi}{\kappa}\,\xi^{\kappa}\right] \tag{32}$$

where

$$\psi = \eta_R\left(\frac{1}{C\gamma_R^2}\right)^{\kappa/2} = \frac{\eta_R}{\xi_R^{\kappa}} \tag{33}$$

and the normalization K is given below

$$K = Q_0\,t_{acc,R}\,\xi_R^{-\kappa}\exp\left[\frac{\eta_R}{\kappa}\left(\frac{\xi_0}{\xi_R}\right)^{\kappa}\right] \tag{34}$$

Like EDD model, the fit parameters of $synconv \otimes n(\xi)$ model for energy dependent acceleration scenario are norm N, κ and ψ. Similarly, N is defined as

$$N = \frac{\delta^3(1+z)}{d_L^2}V\,A\,K\,\sqrt{C} \tag{35}$$

The plot between the difference of the reduced-χ^2 values of the log-parabola and the EDA model vs. reduced-χ^2 values of the log-parabola model (shown in Fig. 6(c)) suggests that the EDA model fits the X-ray spectrum equally well as the log-parabola model. Thus confirming the power of the model to reproduce the curvature in the spectrum. The Spearman's correlation results between the EDA model fit parameters are presented in the last rows of Table 5, and the correlation plots are shown in Fig. 10. The correlations of flux, $F_{0.3-10keV}$ with κ and ψ are nearly similar to the results obtained in the case of energy dependent t_{esc} model. In this case, the r_s (P_s) are obtained as 0.36 ± 0.02 (1.81×10^{-24}) for κ vs. $F_{0.3-10keV}$, and -0.77 ± 0.01 (1.17×10^{-181}) for ψ vs $F_{0.3-10keV}$ respectively. Nevertheless, ψ and κ showed a weak anticorrelation with r_s (P_s) as -0.41 ± 0.01 (2.11×10^{-37}). Now, the relation $\psi = \eta_R\xi_R^{-\kappa}$ implies that $log_{10}\psi$ should be linearly and inversely proportional to κ, which is consistent with the correlation obtained between ψ and κ. Fig. 10(a) shows $log_{10}\psi$ versus κ plot, fitted with a straight line $log_{10}\psi = -0.36\kappa + 0.48$. The result implies that $\eta_R \sim 3.02$ and $\xi_R \sim 2.29$ keV. The variation of the normalization with κ can be represented with the relation given by Equation 35, and can be written as

$$\log N = \frac{\eta_R}{\kappa}\,A^{\kappa} - \kappa\,log\,\xi_R + B \tag{36}$$

The $\log N$ vs. κ plot fitted with the above relation (see Fig. 10(b)) resulting the parameter values as A = 0.15, B = 4.10, and $\eta_R = 3.02$, which provides the value of $\gamma_0 \sim 0.15\,\gamma_R$. Unlike the EDD model, the photon energy corresponding to γ_R is $\xi_R^2 \sim 5.24$ keV which is within the energy range used for the spectral study. Furthermore, γ_0 is not notably smaller than γ_R.

5.3.3 Conclusions

We showed that the energy dependent electron diffusion (EDD) model can also reproduce the spectral curvature. While carrying out the correlation study between the model parameters, we found that N and ψ are strongly anticorrelated with κ, which is consistent with the model prediction. The appropriateness in the observed correlation with the expected one let us estimate the typical photon energy arising from the electron of energy γ_R, as $\xi_R^2 \approx 10.96$ keV and the injection energy of the electron into the acceleration region, as $\gamma_0 \approx 0.045\,\gamma_R$. Similar to the EDD model, EDA model with energy dependent acceleration rate also reproduces the observed X-ray spectrum well and predicts the observed correlation results. In the EDA model, the estimated value of ξ_R^2 is ≈ 5.24 keV, and $\gamma_0 \approx 0.15\,\gamma_R$. Therefore, both the EDD and EDA models provide insight into underlying physical mechanism responsible for X-ray emission. In the earlier work, Hota et al. 2021 had shown similar correlation results between the spectral parameters where they investigated the capability of these models to fit the X-ray observations from a single short-term flare.

In our work, we have probed the spectral feature of Mkn 421 in the energy range 0.3–10 keV using Swift-XRT observations, however, an extended study to hard X-ray is required to understand the role of the considered models better.

Table 5: Spearman Correlation results of the observations with spectral counts ≥ 3000

| Model	Correlation between	r_s	P_s
Log-parabola	α & Flux	-0.81 ± 0.005	4.67×10^{-229}
	β & Flux	0.04 ± 0.02	0.27
	α & N	-0.41 ± 0.008	1.78×10^{-39}
	β & N	0.15 ± 0.02	2.37×10^{-05}
	α & β	-0.21 ± 0.02	7.68×10^{-09}
PL with ξ_{max}	p & Flux	-0.80 ± 0.007	1.92×10^{-209}
	ξ_{max} & Flux	-0.03 ± 0.02	0.44
	p & N	-0.28 ± 0.009	6.31×10^{-19}
	ξ_{max} & N	-0.15 ± 0.02	2.28×10^{-4}
	ξ_{max} & p	0.20 ± 0.02	4.94×10^{-7}
Energy-dependent t_{esc}	κ & Flux	0.32 ± 0.02	3.30×10^{-19}
	ψ & Flux	-0.76 ± 0.008	1.01×10^{-180}
	κ & N	-0.68 ± 0.02	7.95×10^{-114}
	ψ & N	0.70 ± 0.01	2.05×10^{-121}
	ψ & κ	-0.51 ± 0.01	3.65×10^{-51}
Energy-dependent t_{acc}	κ & Flux	0.36 ± 0.02	1.81×10^{-24}
	ψ & Flux	-0.77 ± 0.01	1.17×10^{-181}
	κ & N	-0.78 ± 0.009	9.17×10^{-194}
	ψ & N	0.73 ± 0.004	4.95×10^{-170}
	ψ & κ	-0.41 ± 0.01	2.11×10^{-37}

plots for the difference between the reduced
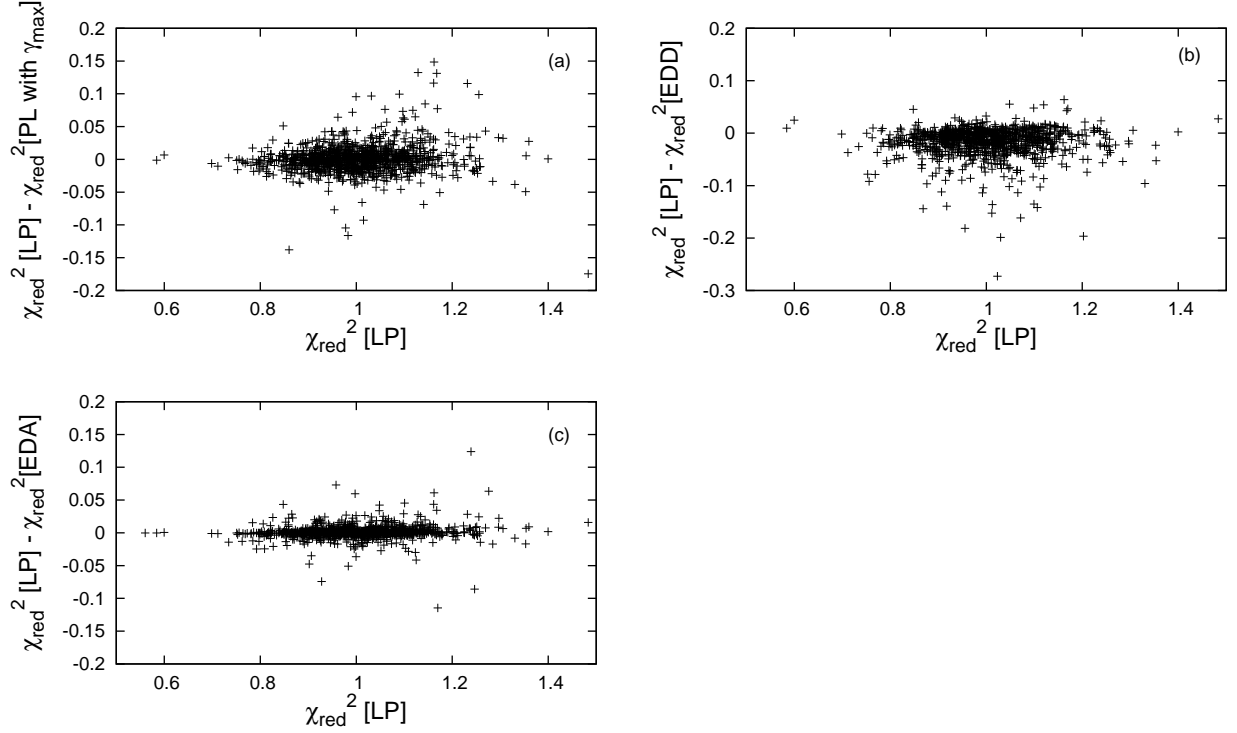
Figure 6: Panels (a-c): plots for the difference between the reduced-χ^2 values of the log-parabola (LP) model to the power-law with ξ_{max}, energy-dependent t_{esc} and the energy-dependent t_{acc} models, vs. the LP model.
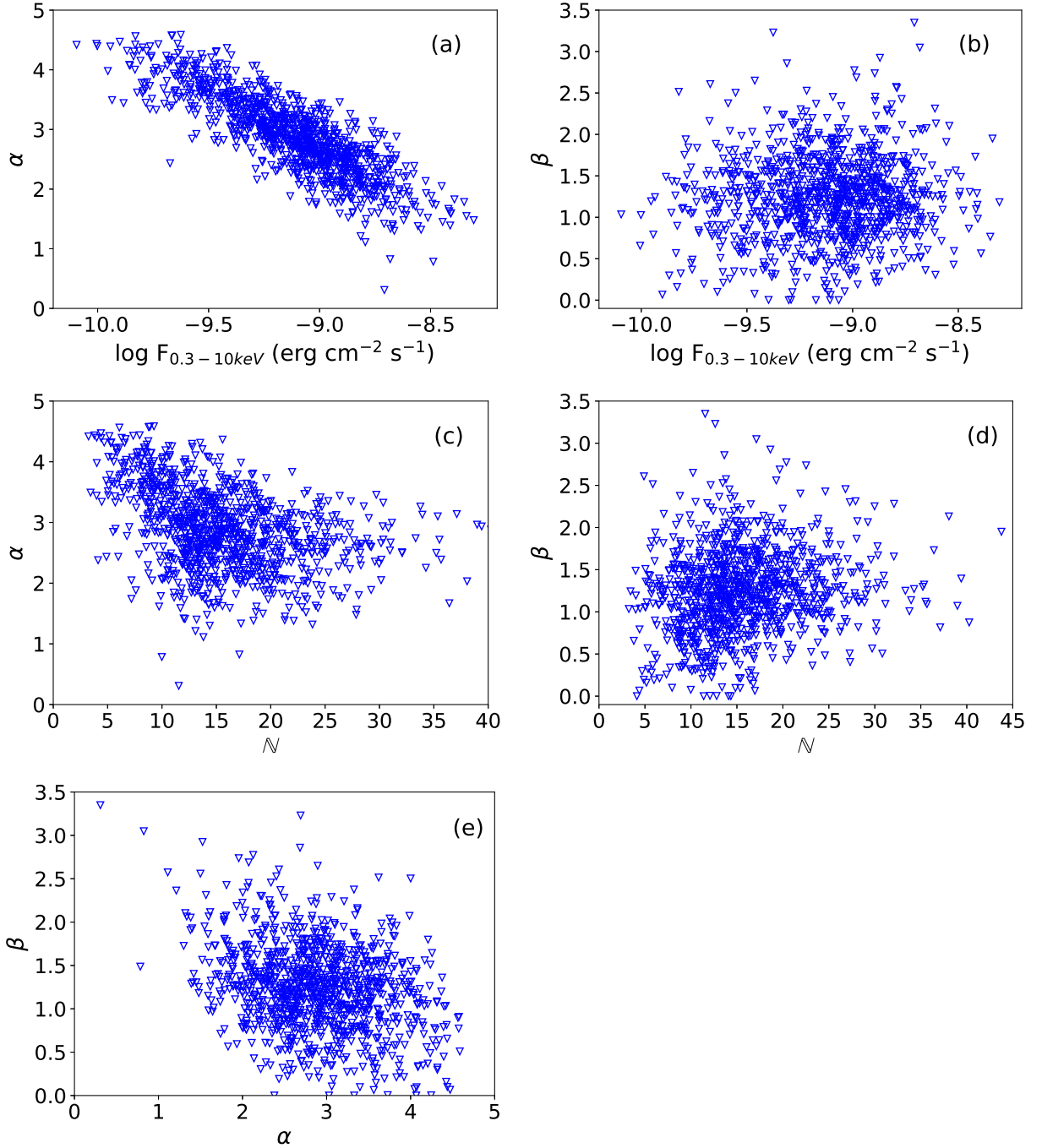
Figure 7: Cross plots of the log-parabola model fit parameters and $F_{0.3-10keV}$. Panels (a-b): α (spectral index) and β (curvature parameter) are plotted vs $F_{0.3-10keV}$. Panels (c-d): α and β are plotted vs normalisation parameter. Panel: β is plotted against α.
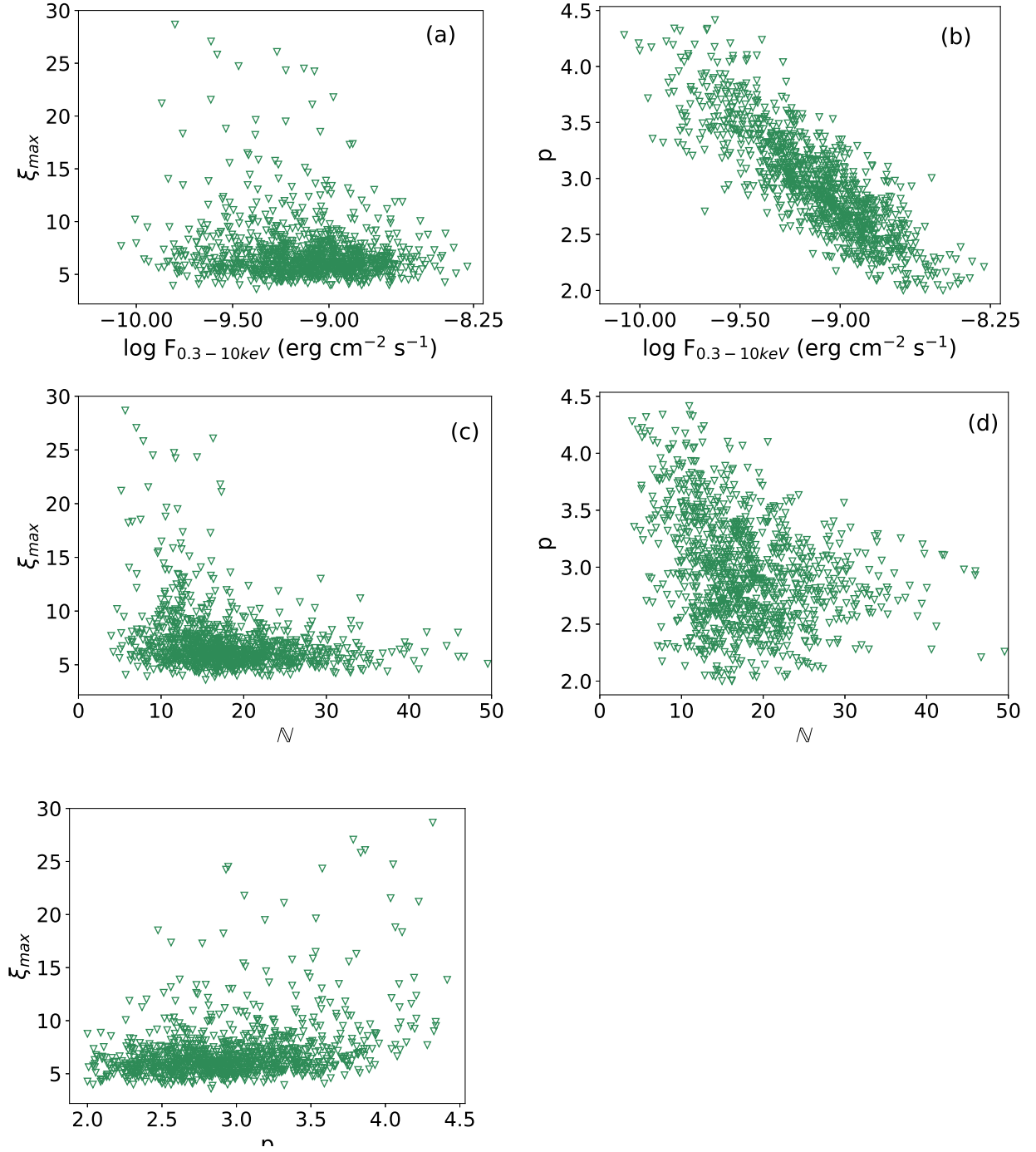
Figure 8: Scatter plots between the power-law with ξ_{max} model fit parameters. Panels (a-b): the maximum energy of electron (ξ_{max}) and the particle spectral index (p) are plotted vs flux, $F_{0.3-10keV}$. Panel (c-d): ξ_{max} and p are plotted vs normalisation. Panel e: ξ_{max} is plotted vs p.
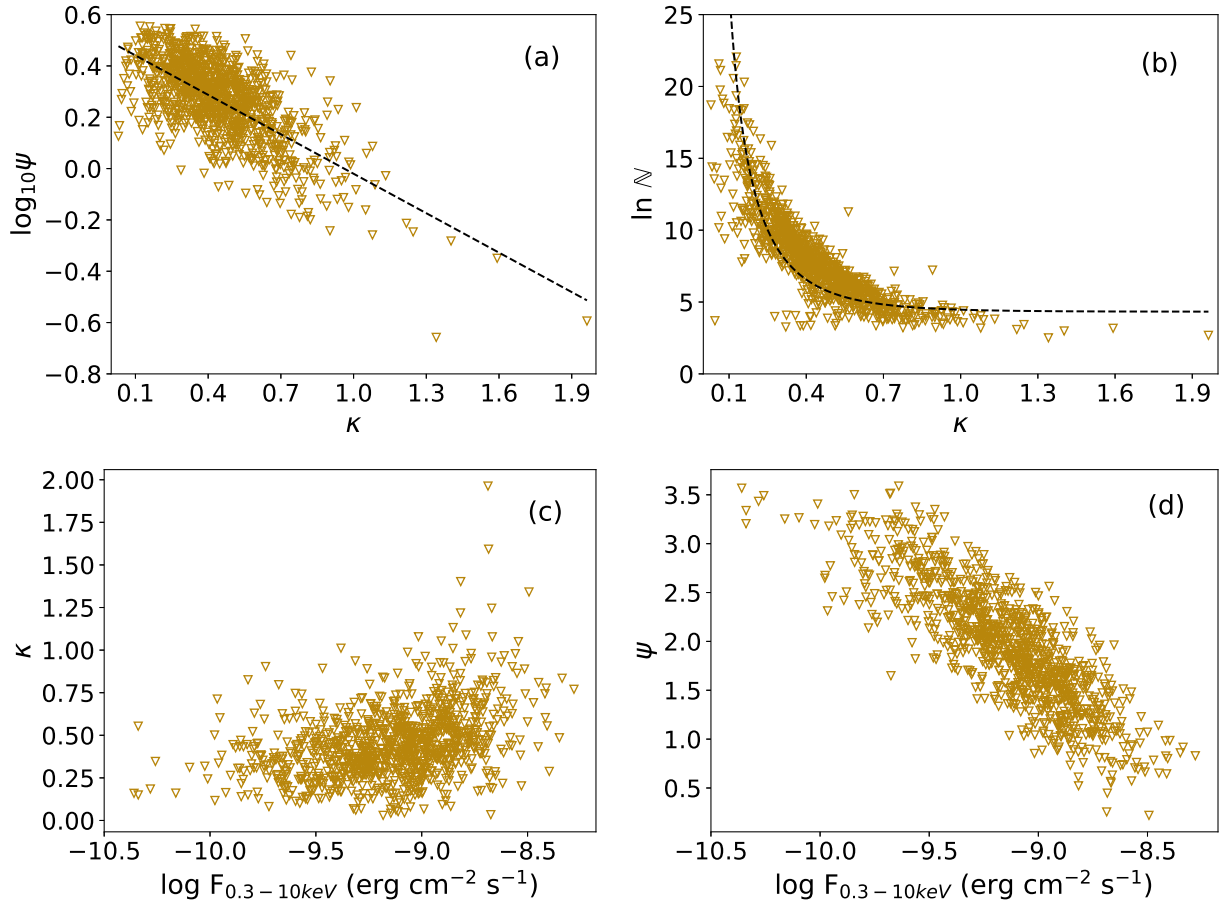
Figure 9: Scatter plots between the energy-dependent t_{esc} model parameters. Panels (a-b): $\log_{10}\psi$ and $\log N$ are plotted vs κ. Panel (c-d): κ and ψ are plotted against flux, $F_{0.3-10keV}$.
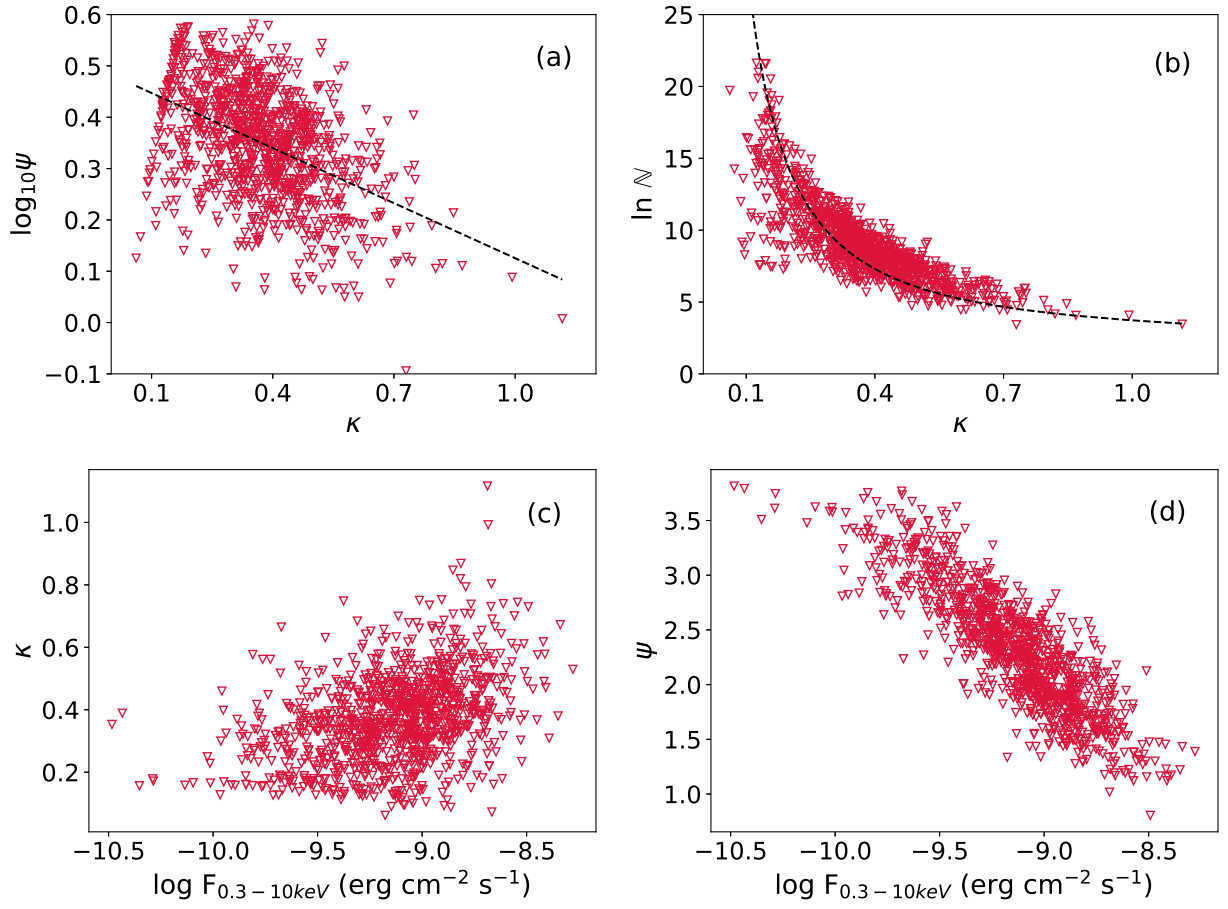
Figure 10: Scatter plots between the energy-dependent t_{acc} model parameters. Panels (a-b): $\log_{10}\psi$ and $\log N$ are plotted vs κ. Panel (c-d): κ and ψ are plotted against flux, $F_{0.3-10keV}$.

Publications

Sinha, A.; Khatoon, R.; Misra, R.; Sahayanathan, S.; Mandal, S.; Gogoi, R.; Bhatt, N., The flux distribution of individual blazars as a key to understand the dynamics of particle acceleration , Monthly Notices of the Royal Astronomical Society Letters 480, L116L120 (5 Pages), 2018.

Khatoon, R.; Shah, Z.; Misra, R.; Gogoi, R., "Study of long-term flux and photon Index distributions of blazars using RXTE observations", Monthly Notices of the Royal Astronomical Society 491, 1934-1940, 2020.

Khatoon, R.; Shah, Z.; Hota, J.; Misra, R.; Gogoi, R., Pradhan, A. C. "Correlations between X-ray spectral parameters of Mkn 421 using long-term Swift-XRT data", Monthly Notices of the Royal Astronomical Society 515, 3749-3759, 2022.

Bibliography

1. Burbidge, G. R. 1959, ApJ, 129, 849

2. Hoyle, F., & Fowler, W. A. 1963, Nature, 197, 533

3. Urry, C. M., & Padovani, P. 1995, PASP, 107, 803

4. Fossati G., Maraschi L., Celotti A., Comastri A., Ghisellini G., 1998, MNRAS, 299, 433

5. Maraschi L., Ghisellini G., Celotti A., 1992, ApJ, 397, L5

6. Fan J. H., 2003, ApJ, 585, L23

7. Uttley P., McHardy I. M., Vaughan S., 2005, MNRAS, 359, 345

8. Negoro H., Mineshige S., 2002, PASJ, 54, L69

9. Quilligan F., McBreen B., Hanlon L., McBreen S., Hurley K. J., Watson D., 2002, AA, 385, 377

10. Giebels B., Degrange B., 2009, AA, 503, 797

11. Chevalier J., Kastendieck M. A., Rieger F. M., Maurin G., Lenain J. P., Lamanna G., 2015, in 34th International Cosmic Ray Conference (ICRC2015). p. 829

12. Sinha A. et al., 2016, AA, 591, A83

13. Kushwaha, P., Chandra, S., Misra, R., et al. 2016, ApJ, 822, L13

14. Shah Z., Mankuzhiyil N., Sinha A., Misra R., Sahayanathan S., Iqbal N., 2018, Research in Astronomy and Astrophysics, 18, 141

15. Aharonian F. et al., 2007, ApJ, 664, L71

16. Narayan R., Piran T., 2012, MNRAS, 420, 604

17. Kirk J. G., Rieger F. M., Mastichiadis A., 1998, AA, 333, 452

18. Sahayanathan S., 2008, MNRAS, 388, L49

19. Kardashev N. S., 1962, Soviet Ast., 6, 317

20. Matsuoka M., et al., 2009, PASJ, 61, 999

21. Sinha A., et al., 2018, MNRAS Letters, 480, L116

22. Punch M. et al., 1992, Nature , 358, 477

23. Wierzcholska A., Wagner S. J., 2016, MNRAS , 458, 56

24. Gaur H., Chen L., Misra R., Sahayanathan S., Gu M. F., Kushwaha P., Dewangan G. C., 2017, ApJ , 850, 209

25. Hota J., Shah Z., Khatoon R., Misra R., Pradhan A. C., Gogoi R., 2021, MNRAS , 508, 5921

26. Kalberla P. M. W., Burton W. B., Hartmann D., Arnal E. M., Bajaja E., Morras R., P ppel W. G. L., 2005, AA , 440, 775

27. Begelman M. C., Blandford R. D., Rees M. J., 1984, Rev. Mod. Phys. , 56, 255

28. Massaro E., Perri M., Giommi P., Nesci R., 2004, AA , 413, 489

29. Massaro F., Tramacere A., Cavaliere A., Perri M., Giommi P., 2008, AA , 478, 395

30. Goswami P., Sahayanathan S., Sinha A., Misra R., Gogoi R., 2018, MNRAS , 480, 2046

31. Kardashev N. S., 1962, Soviet Ast., 6, 317

32. Kirk J. G., Rieger F. M., Mastichiadis A., 1998, AA, 333, 452

FORM-L
UTILISATION CERTIFICATE

COUNCIL OF SCIENTIFIC AND INDUSTRIAL RESEARCH
Human Resource Development Group
CSIR Complex, Library Avenue, Pusa, New Delhi – 110012

CSIR - HRDG Scheme No. : 03(1412)/17/EMR-II

S.No.	Particulars	Letter No. /Bank Transaction ID Nos. & Date	Amount
1	Grants received from CSIR during the year	03(1412)/17/EMR-II dated 09/05/2017	6,87,667/-
2	Unspent balance of previous year	03(1412)/17/EMR-II dated 09/05/2017	Nil
3	Interest earned/accrued on CSIR grant	03(1412)/17/EMR-II dated 09/05/2017	1445/-
		Total	6,89,112/-

1. Certified that out of Rs. **6,87,667/- (Rupees Six Lakhs Eighty Seven Thousand Six Hundred Sixty Seven Only)** of grant-in-aid released by Extramural Research (EMR) Division of HRDG (CSIR) vide letter No./Bank Transaction ID Nos. **03(1412)/17/EMR-II** dated **09/05/2017** as given in the margin during the year **2017 - 2018** and Rs. **1445/-** earned/accrued as interest from bank on grants released by CSIR and Rs. **Nil** on account of unspent balance of the previous year, a sum of Rs. **2,36,958/-*** has been utilized for the purpose for which it was sanctioned and that the balance of Rs. **4,52,154/-*** remaining unutilized at the end of the year has been surrendered to EMR, HRDG (CSIR) (vide letter No. _____ , DD/Cheque No. _____dated _____)/ will be adjusted towards the grant-in-aid payable during the next year.

2. Certified that I have satisfied myself that the conditions on which the grants-in-aid was sanctioned have been duly fulfilled/are being fulfilled and that I have exercised the following checks to see that the money was actually utilized for the purpose for which it was sanctioned. The detail expenditure incurred during the year is shown in the enclosed "Statement of Accounts (Receipt & Payment)".

Page 1 of 2

*Current utilized amount is **Rs. 3,85,796/-** after spending **Rs. 1,48,838.00/-** for Equipment on 25/05/2018.

Current unutilized amount is **Rs. 3,03,316/- after spending **Rs. 1,48,838.00/-** for Equipment on 25/05/2018.

(Kinds of checks exercised)

1. Vouchers and Statement of Accounts
2. Grant-in-Aid
3. Expenditure Register
4. Bank statements for accrual interest

18/06/18	*21/6/18*
Signature of Finance Officer with Date & Seal **Joint Registrar** **Tezpur University**	Countersigned by Registrar of the institute with Date & Seal *Registrar i/c* *Tezpur University*

The Utilization certificate and statement should be signed by Head of the Finance & Accounts and countersigned by Registrar of the University/Institute.

ANNEXURE-II

Consolidated Statement of Accounts
(From the date of commencement 28/07/2017 till 31st March 2018)

Scheme Number : 03(1412)/17/EMR-II

Title of the Research Scheme : **"A Multiwavelength Study of Active Galactic Nuclei and X-ray Sources"**

Name of the Principal Investigator : **Dr. Rupjyoti Gogoi**

Date of Commencement : **28/07/2017**   Date of Termination : Nil

Period (ending 31 March)	Cheque No., date & Amount	Receipts (Particulars of grants received)						Payments (Particulars of grants spent)						
		Stipend	Contingency	Scientist Allowance (for Emeritus Scientist Scheme only)	Equipment Grant	HRA + MA	Total	Stipend	Contingency	Scientist Allowance (for Emeritus Scientist Scheme only)	Equipment Grant	HRA + MA	Total	Balance
From 28/07/2017 to 31/03/2018	Transaction Id: P170926173B 4777 on 26/09/2017 & Amount: 6,87,667/-	3,96,000	91,667	Nil	2,00,000	Nil	6,87,667	97,548	91,110	Nil	48,300*	Nil	2,36,958**	4,50,709***

Signature of Registrar with Stamp
Registrar i/c
Tezpur University

Signature of Finance Officer with Stamp
Joint Registrar
Tezpur University

Signature of PI with Stamp
Rupjyoti Gogoi
Assistant Professor
Deptt. of Physics
Tezpur University

* Additional Amount of **Rs. 1,48,838.00/-** for Equipment has been paid on 25/05/2018 by Tezpur University. So, total Payment under Equipment grant is **Rs. 1,97,138.00/-**.

Total Payment is **Rs. 3,85,796/- as on 25/05/2018 after including payment of Rs. 1,48,838.00/-.

*** **Current balance after paying for equipment** (amount of Rs. 1,48,838.00/-) **is Rs. 3,01,871/-**.

FORM-L

UTILISATION CERTIFICATE

COUNCIL OF SCIENTIFIC AND INDUSTRIAL RESEARCH

Human Resource Development Group

CSIR Complex, Library Avenue, Pusa, New Delhi – 110012

CSIR - HRDG Scheme No. : 03(1412)/17/EMR-II

S.No.	Particulars	Letter No. /Bank Transaction ID Nos. & Date	Amount
1	Grants received from CSIR during the year (2017-2019)	03(1412)/17/EMR-II dated 09/05/2017	6,87,667/-
2	Unspent balance of previous year	03(1412)/17/EMR-II dated 09/05/2017	Nil
3	Interest earned/accrued on CSIR grant (2017-2019)	03(1412)/17/EMR-II dated 09/05/2017	3,975/-
		Total	6,91,642/-

1. Certified that out of Rs. **6,87,667/-** (**Rupees Six Lakhs Eighty Seven Thousand Six Hundred Sixty Seven Only**) of grant-in-aid released by Extramural Research (EMR) Division of HRDG (CSIR) vide letter No./Bank Transaction ID Nos. **03(1412)/17/EMR-II** dated **09/05/2017** as given in the margin during the year **2017 - 2019** and Rs. **3975** earned/accrued as interest from bank on grants released by CSIR and Rs. **Nil** on account of unspent balance of the previous year, a sum of Rs. **6,16,617/-** has been utilized for the purpose for which it was sanctioned and that the balance of Rs. **75,025/-** remaining unutilized at the end of the year has been surrendered to EMR, HRDG (CSIR) (vide letter No.03(1412)/17/EMR-II DD/Cheque No. 433275 dated 28/06/2019)/ will be adjusted towards the grant-in-aid payable during the next year.

2. Certified that I have satisfied myself that the conditions on which the grants-in-aid was sanctioned have been duly fulfilled/are being fulfilled and that I have exercised the following checks to see that the money was actually utilized for the purpose for which it was sanctioned. The detail expenditure incurred during the year is shown in the enclosed "Statement of Accounts (Receipt & Payment)".
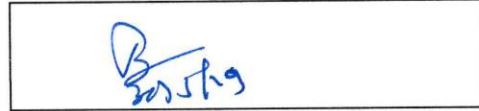
Page 1 of 2

(Kinds of checks exercised)
1. Vouchers and Statement of Accounts
2. Grant-in-Aid
3. Expenditure Register
4. Bank statements for accrual interest

Signature of Finance Officer
with Date & Seal
Finance Officer 30/5/19
Tezpur University

Countersigned by Registrar of the
institute with Date & Seal
Registrar
Tezpur University

The Utilization certificate and statement should be signed by Head of the Finance & Accounts and countersigned by Registrar of the University/Institute.
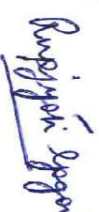
ANNEXURE-II

Consolidated Statement of Accounts

(From the date of commencement 28/07/2017 till 31st March 2019)

Scheme Number : 03(1412)/17/EMR-II

Title of the Research Scheme : "A multiwavelength study of Active Galactic Nuclei and X-ray sources"

Name of the Principal Investigator : Dr. Rupjyoti Gogoi

Date of Commencement : 28/07/2017

Date of Termination : Nil

Period (ending 31 March)	Cheque No., date & Amount	Receipts (Particulars of grants received)						Payments (Particulars of grants spent)						
		Stipend	Contin-gency	Equip-ment Grant	HRA + MA	Interest earned	Total	Stipend	Contin-gency	Equip-ment Grant	HRA + MA	Overhead expenses	Total	Balance
From 28/07/2017 to 31/03/2019	Transaction Id: P170926173 4777 on 26/09/2017 & Amount: 6,87,667/-	3,96,000	91,667	2,00,000	Nil	3,975	6,91,642	2,41,548	1,66,083	1,97,138	Nil	11,848	6,16,617	75,025

HRA from bank (2017-2019)

Signature of Registrar
Tezpur University
with stamp

Signature of Finance Officer
with Stamp
Tezpur University

Signature of PI
with Stamp

Rupjyoti Gogoi
Assistant Professor
Deptt. of Physics
Tezpur University

भारतीय स्टेट बैंक
State Bank of India

आरी करने वाली शाखा
Issuing Branch:TEZPUR
कोड क्र /CODE No: 00195
Tel No: 03712-220592

मांगड्राफ्ट
DEMAND DRAFT

Key: PUCMOZ
Sr. No: 988404

2	8	0	6	2	0	1	9
D	D	M	M	Y	Y	Y	Y

मांगे जानेपर THE DY SECY EXTRAMURAL RESEARC H CSIR COMPLEX*****************

या उनके आदेश पर
OR ORDER

रुपये **RUPEES**MAND PAY

Seventy Five Thousand Twenty Five Only

अदा करें ₹

75025.00

IOI 000525433275   Key: PUCMOZ   Sr. No: 988404   AMOUNT BELOW 75026(7/5)   मूल्य प्राप्त / VALUE RECEIVED

Name of Applicant   TEZPUR UNIVERSITY R& D

प्राधिकृत हस्ताक्षरकर्ता
AUTHORISED SIGNATORY

शाखा प्रबंधक
BRANCH MANAGER

कम्प्यूटर द्वारा मुद्रित होने पर ही वैध   केवल 3 महीने के लिए वैध
VALID ONLY IF COMPUTER PRINTED   VALID FOR 3 MONTHS ONLY

भारतीय स्टेट बैंक
STATE BANK OF INDIA
अदाकर्ता शाखा / DRAWEE BRANCH:MICR CP CENTRE
कोड क्र . /CODE No: 04328

₹ 1,50,000/- एवं अधिक के लिखत दो अधिकारियों द्वारा हस्ताक्षरित होने पर ही वैध है ।
INSTRUMENTS FOR ₹ 1.50 LAC & ABOVE ARE NOT VALID UNLESS SIGNED BY TWO OFFICERS

"433275" 000002000: 000525" 16

Abdul Hannan
H - 1021

FORM-L
UTILISATION CERTIFICATE

COUNCIL OF SCIENTIFIC AND INDUSTRIAL RESEARCH
Human Resource Development Group
CSIR Complex, Library Avenue, Pusa, New Delhi – 110012

CSIR - HRDG Scheme No. : 03(1412)/17/EMR-II

S.No.	Particulars	Letter No. /Bank Transaction ID Nos. & Date	Amount
1	Grants received from CSIR during the year (2019-2020)	03(1412)/17/EMR-II dated 09/05/2017	5,29,000/-
2	Unspent balance of previous year	03(1412)/17/EMR-II dated 09/05/2017	Nil
3	Interest earned/accrued on CSIR grant	03(1412)/17/EMR-II dated 09/05/2017	Nil *
		Total	5,29,000/-

* The grants for the period from 01/04/2019 to 31/03/2020 was received on 19/08/2020 (after the financial year), therefore Interest from bank on grants received from CSIR is Nil.

1. Certified that out of Rs. **5,29,000/-** (Rupees Five Lakhs Twenty Nine Thousand Only) of grant-in-aid released by Extramural Research (EMR) Division of HRDG (CSIR) vide letter No./Bank Transaction ID Nos. **03(1412)/17/EMR-II** dated **09/05/2017** as given in the margin during the year **2019 - 2020** and Rs. **Nil** earned/accrued as interest from bank on grants released by CSIR and Rs. **Nil** on account of unspent balance of the previous year, a sum of Rs. **4,29,000** /- has been utilized for the purpose for which it was sanctioned and that the balance of Rs. **100,000** remaining unutilized at the end of the year has been surrendered to EMR, HRDG (CSIR) (vide letter No. _X___ _x__ , DD/Cheque No. _X__ _x___ dated ___x___ _x___)/ will be adjusted towards the grant-in-aid payable during the next year.

2. Certified that I have satisfied myself that the conditions on which the grants-in-aid was sanctioned have been duly fulfilled/are being fulfilled and that I have exercised the following checks to see that the money was actually utilized for the purpose for which it was sanctioned. The detail expenditure incurred during the year is shown in the enclosed "Statement of Accounts (Receipt & Payment)".

Page 1 of 2

(Kinds of checks exercised)
1. Vouchers and Statement of Accounts
2. Grant-in-Aid
3. Expenditure Register
4. Bank statements for accrual interest

Signature of Finance Officer
Finance Officer
with Date & Seal
Tezpur University

Countersigned by Registrar of the
institute with Date & Seal
Registrar
Tezpur University

The Utilization certificate and statement should be signed by Head of the Finance & Accounts and countersigned by Registrar of the University/Institute.

ANNEXURE-II

Consolidated Statement of Accounts
(From 01/04/2019 to 31/03/2020)

Scheme Number : **03(1412)/17/EMR-II**

Title of the Research Scheme : **"A multiwavelength study of Active Galactic Nuclei and X-ray sources"**

Name of the Principal Investigator : **Dr. Rupjyoti Gogoi**

Date of Commencement : **28/07/2017**

Date of Termination : Nil

Period (ending 31 March)	Cheque No., date & Amount	Receipts (Particulars of grants received)						Payments (Particulars of grants spent)						Balance
		Stipend	Contin-gency	Scientist Allowance (for Emeritus Scientist Scheme only)	Equip-ment Grant	HRA + MA	Total	Stipend	Contin-gency	Scientist Allowance (for Emeritus Scientist Scheme only)	Equip-ment Grant	HRA + MA	Total	
From 01/04/2019 to 31/03/2020	Transaction Id: P20081975762595 on 19/08/2020 & Amount: 5,29,000/-	4,29,000	1,00,000	Nil	Nil	Nil	5,29,000	4,29,000	Nil	Nil	Nil	Nil	4,29,000	1,00,000

Signature of Registrar with Stamp

Tezpur University

Signature of Finance Officer with Stamp

Signature of PI with Stamp

Assistant Professor
Dept. of Physics
Tezpur University

UTILISATION CERTIFICATE

COUNCIL OF SCIENTIFIC AND INDUSTRIAL RESEARCH
Human Resource Development Group
CSIR Complex, Library Avenue, Pusa, New Delhi – 110012

CSIR - HRDG Scheme No. : 03(1412)/17/EMR-II

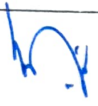| S.No.	Particulars	Letter No. /Bank Transaction ID Nos. & Date	Amount
1	Grants received from CSIR during the year (01/04/2020-27/07/2020)	Nil	1,00,000.00 (Opening balance of Rs. 100000)
2	Interest earned/accrued on CSIR grant	--	1563.00
3	Amount utilized during 01/04/2020-31/03/2021	--	Nil
4	Unspent balance as on 31/03/2021 [(1)+(2)-(3)]	--	1,01,563.00

1. Certified that out of Rs. **Nil** of grant-in-aid released by Extramural Research (EMR) Division of HRDG (CSIR) and opening balance of **Rs. 1,00,000/** as mentioned in the table given above for the time duration 01/04/2020-27/07/2020 and **Rs. 1563/** earned/accrued as interest from bank on grants released by CSIR , a sum of Rs. **Nil** has been utilized for the purpose for which it was sanctioned and that the balance of Rs. 101563/ remaining unutilized at the end of the year has been surrendered to EMR, HRDG (CSIR) (vide DD No. _____ dated _____).

2. Certified that I have satisfied myself that the conditions on which the grants-in-aid was sanctioned have been duly fulfilled/are being fulfilled and that I have exercised the following checks to see that the money was actually utilized for the purpose for which it was sanctioned. The detail expenditure incurred during the year is shown in the enclosed "Statement of Accounts (Receipt & Payment)".

(Kinds of checks exercised)
  1. Vouchers and Statement of Accounts
  2. Grant-in-Aid

3. Expenditure Register
4. Bank statements for accrual interest

<table>
<tr><td>Finance Officer
Tezpur University
Signature of Finance Officer
with Date & Seal</td><td>Registrar
Tezpur University
Countersigned by Registrar of the
institute with Date & Seal</td></tr>
</table>

The Utilization certificate and statement should be signed by Head of the Finance & Accounts and countersigned by Registrar of the University/Institute.

Consolidated Statement of Accounts
(From 01/04/2020 till 31st March 2021)

Scheme Number : 03(1412)/17/EMR-II

Title of the Research Scheme : "A multiwavelength study of Active Galactic Nuclei and X-ray sources"

Name of the Principal Investigator : **Dr. Rupjyoti Gogoi**

Date of Commencement : **28/07/2017**

Date of Termination : **31/12/2021**

		Receipts (Particulars of grants received)						Payments (Particulars of grants spent)						
Period (ending 31 March)	Cheque No., date & Amount	Stipend	Contin-gency	Scientist Allowance (for Emeritus Scientist Scheme only)	Equip-ment Grant	HRA+ MA	Total	Stipend	Contin-gency	Scientist Allowance (for Emeritus Scientist Scheme only)	Equip-ment Grant	HRA + MA	Total	Balance
From 01/04/2020 to 31/03/2021	NA	Nil	Nil	Nil	Nil	Nil	101563/- (unspent balance + interest)	Nil	Nil	Nil	Nil	Nil	Nil	101563/-

Signature of Registrar with Stamp

Registrar
Tezpur University

Signature of Finance Officer with Stamp

Finance Officer
Tezpur University

Signature of PI with Stamp

भारतीय स्टेट बैंक
STATE BANK OF INDIA

Issuing Branch:TEZPUR UNIVERSITY
कोड नं./CODE No: 14259
Tel No. 03712-267285

A/C Payee

मांगड्राफ्ट
DEMAND DRAFT

Key: TAGJAN
Sr. No: 186975

1	2	0	5	2	0	2	3
D	D	M	M	Y	Y	Y	Y

मांगे जानेपर DEPUTY SECRETARY, EXTRAMURAL RESEARCH, CSIR*****************   या उनके आदेश पर

ON DEMAND PAY   OR ORDER

रुपये RUPEES   One Lakh One Thousand Five Hundred and Sixty Three Only

अदा करें   ₹   101563.00

IOI 000536847197   Key: TAGJAN   Sr. No: 186975   AMOUNT BELOW 101564(0/6)   मूल्य प्राप्त / VALUE RECEIVED
Name of Applicant   TEZPUR UNIVERSITY R& D

भारतीय स्टेट बैंक
STATE BANK OF INDIA
अदाकर्ता शाखा / DRAWEE BRANCH:NEW DELHI MAIN BRANCH
कोड नं. /CODE No: 00691

प्राधिकृत हस्ताक्षरकर्ता
AUTHORISED SIGNATORY
₹1,50,000/- एवं अधिक के लिखत में दो अधिकारी
INSTRUMENTS FOR ₹ 1,50,000/- & ABOVE ARE NOT VALID UNLESS SIGNED BY TWO OFFICERS

Bhaskardeep Das
D-8347

कम्प्यूटर द्वारा मुद्रित होने पर ही वैध
VALID ONLY IF COMPUTER PRINTED

केवल 3 महीने के लिए वैध
VALID FOR 3 MONTHS ONLY

SESHASAH(D) / CTS-2010

⑈847197⑈ 000002000⑈ 000536⑈ 16